∂A Pan-African Convection-Permitting Regional Climate Simulation with the Met Office Unified Model: CP4-Africa

Rachel A. Stratton, Catherine A. Senior, and Simon B. Vosper

Met Office, Exeter, United Kingdom

Sonja S. Folwell

Centre for Ecology and Hydrology, Wallingford, United Kingdom

Ian A. Boutle, Paul D. Earnshaw, Elizabeth Kendon, Adrian P. Lock,
Andrew Malcolm, James Manners, Cyril J. Morcrette,
Christopher Short, and Alison J. Stirling

Met Office, Exeter, United Kingdom

Christopher M. Taylor

Centre for Ecology and Hydrology, Wallingford, United Kingdom

Simon Tucker, Stuart Webster, and Jonathan M. Wilkinson

Met Office, Exeter, United Kingdom

ABSTRACT

A convection-permitting multiyear regional climate simulation using the Met Office Unified Model has been run for the first time on an Africa-wide domain. The model has been run as part of the Future Climate for Africa (FCFA) Improving Model Processes for African Climate (IMPALA) project, and its configuration, domain, and forcing data are described here in detail. The model [Pan-African Convection-Permitting Regional Climate Simulation with the Met Office UM (CP4-Africa)] uses a 4.5-km horizontal grid spacing at the equator and is run without a convection parameterization, nested within a global atmospheric model driven by observations at the sea surface, which does include a convection scheme. An additional regional simulation, with identical resolution and physical parameterizations to the global model, but with the domain, land surface, and aerosol climatologies of CP4-Africa, has been run to aid in the understanding of the differences between the CP4-Africa and global model, in particular to isolate the impact of the convection parameterization and resolution. The effect of enforcing moisture conservation in CP4-Africa is described and its impact on reducing extreme precipitation values is assessed. Preliminary results from the first five years of the CP4-Africa simulation show substantial improvements in JJA average rainfall compared to the parameterized convection models, with most notably a reduction in the persistent dry bias in West Africa, giving an indication of the benefits to be gained from running a convection-permitting simulation over the whole African continent.

Corresponding author: Rachel Stratton, rachel.stratton@metoffice.gov.uk

1. Introduction

The Future Climate for Africa (FCFA) Improving Model Processes for African Climate (IMPALA) project aims to deliver a step change in global climate model capability for Africa by delivering reductions in model

systematic errors through improved understanding and representation of the drivers of African climate and hence reducing uncertainty in future projections. This ambitious project has chosen to focus on a single model, the Met Office Unified Model (UM), so there is rapid pull-through into improved model performance, while delivering new metrics and understanding to the broader science community. One of the key challenges to improved performance is a better understanding of how the fundamentals of convective parameterization impact on African climate variability and change. Crucially for IMPALA, we are able to address this challenge through the power of the seamless UM system (Cullen 1993; Brown et al. 2012) to provide high-resolution simulations representing individual convective cloud systems on an Africa-wide domain for the first time. Within the project we will deliver two 10-yr simulations with a 4.5-km horizontal grid spacing on a pan-African domain for the present day (1997–2007) and for an idealized future climate (details will be provided in a future paper). This paper describes the design, domain, and forcing of the present-day experiments and first results from the early years of this simulation.

The configuration of the Pan-African Convection-Permitting Regional Climate Simulation with the Met Office Unified Model (CP4-Africa) builds on work within the Cascade project (Pearson et al. 2010; Marsham et al. 2011), which ran 1.5-, 4-, and 12-km horizontal resolution convection-permitting simulations using older configurations of the UM over West Africa for a period in 2006, as part of the African Monsoon Multidisciplinary Analysis (AMMA) period (Redelsperger et al. 2006) and compared the results with those from simulations at 12 km and a global 40-km horizontal resolution using convection parameterization. These studies, together with a review of regional convection-permitting climate modeling (Prein et al. 2015), show a clear benefit of 4-km resolution over the global (40 km) and regional (12 km) models running with convective parameterizations.

At a 4-km scale, models can resolve larger storms and mesoscale convective organization (typically scales of greater than 100 km; Houze 2004) explicitly on the model grid but convective plumes, small showers, and shallow clouds are still not resolved. Marsham et al. (2013), Pearson et al. (2014), Birch et al. (2014b), Birch et al. (2014a), and Stein et al. (2015) showed that convection-permitting models were better able to simulate the diurnal cycle of tropical convection over land, the vertical structure of clouds, the coupling between moist convection and convergence, the water budget, and the continental-scale flow. Failure to model the correct diurnal cycle of deep convection and associated cold pools contributes to errors in winds over the Sahara

(Garcia-Carreras et al. 2013) and problems with modeling dust (Marsham et al. 2011). Both of these aspects are improved in the convection-permitting simulations. A study of the relationship between soil moisture and convection (Taylor et al. 2013) showed that the global model does not have the correct feedback between soil moisture and convection whereas the convection-permitting models are capable of representing this. The expectation from the Cascade project is that a simulation with a 4.5-km horizontal grid spacing will improve many of the known model biases within a global model running with a convective parameterization scheme, giving a better simulation of the day-to-day variability of precipitation over the African continent. A realistic simulation of this variability is very important for studies concerned with climate change over Africa and its impact on water resources, agriculture, and weather-related hazards such as flooding.

Versions of the convection-permitting UM are routinely used at the Met Office to produce regional operational forecasts over the United Kingdom [U.K.-Wide Variable Horizontal Resolution Model (UKV), with 1.5-km grid spacing; Lean et al. 2008], Europe (4.4 km), Lake Victoria (4 km; Chamberlain et al. 2014) and Southeast Asia (4 km). While these models give better guidance than the operational global model (run with convective parameterization), there are still problems. The time of the diurnal cycle of convection over land is better but it is still not in complete agreement with the observations. Over the sea, tropical convection can be slow to initiate. Over both land and sea the convection is often referred to as being too "blobby" (i.e., circular areas of high precipitation rates rather than large randomly shaped areas of precipitation with high and low values).

Earlier versions of the convection-permitting model have been used for climate studies over the United Kingdom (1.5 km) (Kendon et al. 2014) and a region surrounding Singapore (4.5 km) (Birch et al. 2016). To date, climate projections over Africa have been provided using non-convection-permitting global or regional models typically running at resolutions of 50 km [e.g., IPCC Fifth Assessment Report (AR5; Niang et al. 2014) or the Coordinated Regional Downscaling Experiment for Africa (CORDEX-Africa; Laprise et al. 2013)]. The FCFA IMPALA project for the first time will run climate-length simulations with a convection-permitting model for the African continent.

Section 2 describes the model and section 3 the experimental design. Section 4 provides results from two sensitivity studies looking at the impact of changes to CP4-Africa, which have not been well tested before. The first study involves the inclusion of a scheme to enforce moisture conservation, and the second study is the
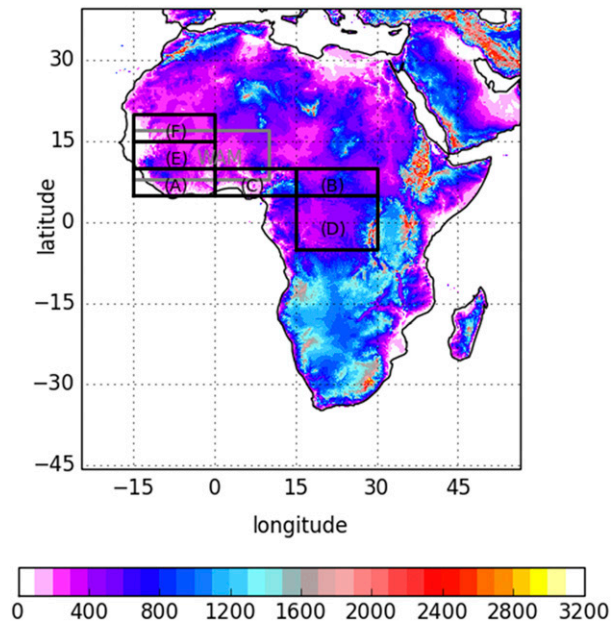
FIG. 1. Map showing orography (terrain heights; m) and the region of CP4-Africa. The plot also shows different regions of Africa used for subsequent analysis. (Regions A–F are used for diurnal cycle analysis in Fig. 12.)

addition of stochastic perturbations to the boundary layer to promote the development of explicitly resolved eddies, which subsequently grow into convective clouds. A non-convection-permitting regional simulation (R25-Africa) using identical resolution and physical parameterizations to the N512L85-resolution global model but the domain, land surface, and aerosol climatologies of CP4-Africa have been run to aid in our understanding of the differences between the CP4-Africa and global model. Preliminary results from the first five years of the CP4-Africa simulation and comparisons with equivalent results from the R25-Africa regional and N512L85-resolution global models are presented in section 5. A summary is provided in section 6.

2. Model description

CP4-Africa is based on the Met Office UKV regional model, which has been in use for operational numerical weather prediction since 2012 (Clark et al. 2016; see appendix B for model availability). The UKV is a U.K.-wide model with variable horizontal resolution (Tang et al. 2013), with a 1.5-km uniform horizontal grid over the central U.K. area, but with the grid spacing outside this area stretching to 4 km at the boundaries. CP4-Africa uses a fairly uniform horizontal grid spacing (from 3.2 km east–west at 45°S to 4.5 km at the equator and north–south) and covers the whole of Africa (Fig. 1),

resolving many inland lakes and mountain ranges. This section describes the dynamics and physics used in the 4.5-km model and points to the differences between the driving N512L85-resolution global model and the R25-Africa regional model.

The choice of resolution for CP4-Africa is the result of a compromise between the domain size required to include the entire continent and the computational cost. Table 1 provides the dimensions of both the CP4-Africa and R25-Africa regional models. To reduce undesirable effects from lateral boundaries on cyclonic weather systems over southern Africa, the southern boundary is chosen to be as distant as possible from the tip of Africa.

With a 4.5-km grid spacing we can expect CP4-Africa to partially resolve deep convection but not smaller-scale congestus or shallow convection. Hence, in regions where shallow convection is a dominant process the model performance may be suboptimal. It should also be noted that no attempt has been made to optimize the model performance specifically for Africa (e.g., by tuning the physical parameterizations).

a. Dynamics and grid

The UM is a nonhydrostatic model with a deep-atmosphere formulation based on a semi-implicit semi-Lagrangian dynamical core. The driving global model and both regional configurations employed here are based on Even Newer Dynamics for General Atmospheric Modeling of the Environment (ENDGame) dynamics (Wood et al. 2014). ENDGame employs an iterative approach to the semi-implicit time step, resulting in better coupling to the model physics and improved numerical stability than in the previous dynamical core [New Dynamics; Davies et al. 2005], which suffered from some stability problems within the Cascade project (Pearson et al. 2010). The global model ensures conservation of dry and moist mass using a global correction scheme (Zerroukat 2010). CP4-Africa uses a similar scheme (Aranami et al. 2015) developed specifically for regional models, where the mass flux through lateral boundaries must be accounted for in the budget calculation. The importance of including this scheme in CP4-Africa is discussed in section 4a. R25-Africa was run without the regional dry and moist mass conservation scheme.

The UM uses a latitude–longitude grid with an Arakawa C grid staggering in the horizontal and hybrid height coordinate with a Charney–Phillips staggering in the vertical. The vertical grid for CP4-Africa consists of 80 levels with the model top placed at 38.5 km. The grid is stretched to provide finer resolution in the boundary layer and troposphere and contains more levels in the upper troposphere than are typically used in midlatitude configurations (e.g., UKV) in order to better resolve

TABLE 1. The grid details and model time steps for the CP4-Africa and R25-Africa regional models and the driving global model.

Quantity	CP4-Africa (4.5 km)	R25-Africa	Global
No. of rows	2100	366	768
No. of columns	2000	236	1024
No. of model levels	80	63	85
Model top (km)	38.5	41.0	85.0
Lowest wind level over sea (m)	2.5	10.0	10.0
Lowest temp level over sea (m)	5.0	20.0	20.0
No. of levels below 5 km	32	26	26
No. of levels below 16 km	56	47	47
Northern lat	39.505°N	39.844°N	90.0°N
Southern lat	45.525°S	45.820 305°S	90.0°S
Lat spacing	0.0405°	0.234 375°	0.234 375°
Lat spacing (km)	4.5	26.0	26.0
Western lon	24.5°W	25.489°W	0.0°
Eastern lon	56.48°E	57.3°E	360.0°
Lon spacing	0.0405°	0.351 562°	0.351 562°
Lon spacing at equator (km)	4.5	39.0	39.0
Time step (s)	100 (75)	600	600

tropical convection and the deeper tropical troposphere. The lowest grid levels over the sea are 2.5 m for horizontal winds and 5 m for temperature and moisture, decreasing to 0.6 and 1.1 m, respectively, over the highest terrain (4592 m). The vertical grid spacing increases quadratically with height. There are 32 levels in the lowest 5 km, and 56 levels below 16 km. Grid spacing at heights of approximately 100 m, 1 km, 5 km, and 16 km above sea level are approximately 40, 140, 300, and 590 m, respectively. The extra vertical resolution of CP4-Africa relative to R25-Africa (see Table 1) is mainly in the lowest 5 km. The exact impact of this increase in resolution is unknown. Attempts have been made to make the model physics schemes as insensitive to vertical resolution as possible, but more levels will tend to contribute to differences in the interaction of clouds and radiation.

The CP4-Africa model time step was initially set to 100 s, but was subsequently reduced to 75 s (see section a in appendix A). The change in time step is not expected to have a significant impact on the simulation. CP4-Africa includes graupel as a prognostic variable in addition to the moist variables of water vapor, cloud liquid, cloud ice, and rain used by the global model and R25-Africa simulations.

b. Physical parameterization

CP4-Africa does not include a convection parameterization and relies on the model dynamics to explicitly represent convective clouds. Clearly convection will be poorly resolved on a 4.5-km grid, but in the current absence of a scale-aware convection scheme that correctly parameterizes subgrid convective motion and

hands over to the model dynamics for clouds larger than the model filter scale, this is a pragmatic choice made based on previous evidence that the removal of the parameterization will result in more realistic behavior (e.g., Birch et al. 2014b; Taylor et al. 2013). It is also worth noting that this approach is different from that of the Cascade project, whose 4-km Africa simulations did use a version of the UM convection scheme, but with a grid-length-scaled CAPE closure that in practice severely restricted the time step increments from deep convection.

The UM includes a comprehensive suite of physical parameterization schemes that are designed for seamless use across global NWP and climate configurations and hence in the N512L85-resolution global model and R25-Africa climate configurations. Many of these parameterizations are also used in convection-permitting regional versions of the model, with the obvious exception of the convection scheme. Table 2 gives a quick summary of the other main differences in the physics schemes used in the CP4-Africa, R25-Africa, and N512L85-resolution global model configurations. The parameterizations used in CP4-Africa can be summarized as follows:

- Radiation parameterization—The radiative transfer scheme of Edwards and Slingo (1996) is used with a configuration similar to that described by Walters et al. (2011) but with several upgrades. These include improvements to the ice cloud optical properties, representation of orographic slope, shading and sky-view effects (Manners et al. 2015), and computationally efficient treatment of scattering (Manners et al. 2012). Aerosol absorption and scattering assumes

TABLE 2. Summary of the major differences in the physics and surface forcing for the CP4-Africa and R25-Africa regional models and the driving global model.

Quantity	CP4-Africa (4.5 km)	R25-Africa	Global
Convective parameterization	No	Yes, same as global	Yes
Radiation scheme	Edwards–Slingo	Edwards–Slingo	Edwards–Slingo
Period of full radiation calculation (min)	15	60	60
Substepped corrections due to cloud (min)	5	None	None
Aerosols and ozone	Climatology	Climatology	Interactive U.K. Chemistry and Aerosols model (UKCA)
Large-scale cloud scheme	Smith scheme	PC2	PC2
Cloud microphysics	Wilson and Ballard	Wilson and Ballard	Wilson and Ballard
Subgrid turbulent production of mixed-phase cloud	No	Yes	Yes
Source of cloud droplet No. concentration	Aerosol climatology	Aerosol climatology	Interactive UKCA aerosols
Microphysics time step (s)	100 (75)	120	120
Includes graupel?	Yes	No	No
Lightning diagnosis	Yes	No	No
Boundary layer scheme	Blended scheme	No blending	No blending
Stochastic perturbations to boundary layer?	Yes	No	No
Frictional heating from turbulent dissipation?	No	Yes	Yes
Orogaphic drag scheme?	Yes	Yes	Yes
Land and sea surface scheme	JULES, nine tiles	JULES, nine tiles	JULES, nine tiles
Land-surface type and properties	Sandy soil	Sandy soil	Varied soil
JULES land settings	As in R25-Africa	Close to GL7	GL7
JULES sea settings	As in UKV	GL7	GL7
Hydrology scheme	PDM scheme	PDM scheme	TOPMODEL
Vegetation cover data	CCI-LC	CCI-LC	IGBP land cover
SST	Reynolds	Reynolds	Reynolds
Lake surface temp	ARC-Lake	ARC-Lake	GISST
Moisture conservation	New regional version	None	Global version
Simulation start–end dates	1 Jan 1997–1 Mar 2007	1 Jan 1997–1 Mar 2007	1 Sep 1988–1 Dec 2010

climatological aerosol properties. Trace greenhouse gases are included with time-varying but spatially uniform mixing ratios. A climatological three-dimensional ozone field is prescribed; see section 3c. Full radiation calculations are made every 15 min, with substepped corrections due to cloud evolution performed every 5 min.

- Large-scale cloud parameterization—At all but the very highest (less than 1 km horizontal) resolutions clouds will form in reality before the grid-box mean humidity reaches saturation. A parameterization of subgrid cloud variability is therefore required. Global UM configurations and R25-Africa use a prognostic cloud fraction and condensation (PC2; Wilson et al. 2008) scheme whereas CP4-Africa, like other convection-permitting UM formulations, uses the diagnostic Smith (1990) scheme. This diagnoses the liquid cloud fraction and condensed water when the grid-box mean relative humidity exceeds a critical value (RHcrit). Ice water content is forecast by the microphysics scheme and fractions diagnosed from this as in Abel et al. (2017). Phase changes release latent heat, and the

fractional cloud cover and liquid and ice water content are passed to the cloud microphysics and radiation schemes. The radiative impact of thin liquid clouds that do not fill the entire depth of a model layer follows a similar approach to that described by Boutle and Morcrette (2010) in which the cloud scheme is applied to sublayers.

- Cloud microphysics parameterization and lightning diagnosis—The treatment of cloud microphysical processes is based on Wilson and Ballard (1999), with extensive modifications described in Walters et al. (2017b, manuscript submitted to Geosci. Model Dev., hereafter WGMD). Additionally, the warm-rain scheme now includes the effect of subgrid variability on microphysical process rates, as described in Boutle et al. (2014a), and the ice particle size distribution of Field et al. (2007) is used. A prognostic mass mixing ratio for graupel is included, following Forbes and Halliwell (2003). This represents a second category of ice with higher densities and fall speeds found in convective cloud. The prognostic graupel is also a prerequisite for the inclusion of a lightning flash rate

prediction scheme. This scheme is described by McCaul et al. (2009), and has been shown to produce useful forecasts in convection-permitting forecasts (Wilkinson and Bornemann 2014). A nonadvected climatological-mean aerosol (section 3c) is used to generate the cloud droplet number concentration. Following the methodology of Wilkinson et al. (2013), the cloud droplet number concentration is exponentially reduced at altitudes below 150 m to match observations of droplet number concentration in fog events.

- Boundary layer turbulence parameterization—The parameterization of turbulence in convection-permitting models requires special treatment because, although most turbulent motions are still unresolved, the largest scales can be of a similar size to the grid length. The model must therefore be able to parameterize the smaller scales, resolve the largest ones if possible, and not alias turbulent motions smaller than the grid scale onto the grid scale. CP4-Africa uses the "blended" boundary layer parameterization (Boutle et al. 2014b) to achieve this. This scheme transitions from the one-dimensional vertical scheme of Lock et al. (2000), suitable for low-resolution simulations, to a three-dimensional turbulent mixing scheme based on Smagorinsky (1963) and suitable for high-resolution simulations, with a weighting that is a function of the ratio of the grid length to a turbulent length scale. The blended eddy diffusivity, including any nonlocal contribution from the Lock et al. (2000) scheme, is applied to downgradient mixing in all three dimensions, while appropriately weighted nonlocal fluxes of heat and momentum are retained in the vertical for unstable boundary layers. Turbulent form drag from unresolved orography is parameterized via an effective roughness length scheme (e.g., Wood and Mason 1993) whereby the vegetative roughness is enhanced to represent the surface pressure drag due to the subgrid terrain.

- Stochastic perturbations—To improve the triggering of resolved convection, stochastic perturbations to temperature and moisture are applied in the subcloud layer of cumulus-capped convective boundary layers [diagnosed following Lock et al. (2000)]. Designed to represent realistic variability resulting from large boundary layer eddies, the perturbation scale χ_* (where χ is either the potential temperature or specific humidity) is taken as $\chi_* = \overline{w'\chi'}|_s/w_m$, where $\overline{w'\chi'}|_s$ is the surface turbulent flux of χ, and the turbulence velocity scale w_m is given by $w_m^3 = u_*^3 + c_{ws}w_*^3$. Here, u_* is the friction velocity, and w_* is the convective velocity scale, with $c_{ws} = 0.25$. Finally, χ_* is constrained to be positive and less than 1 K or 10% of the specific humidity. In the vertical χ_* is scaled by an empirical piecewise linear "shape" function equal to unity in the middle of the boundary layer and zero at the surface and top of the subcloud layer. Loosely based on Muñoz-Esparza et al. (2014), the random number field underlying the perturbations is held constant over eight grid-length squares in the horizontal and is updated in time following McCabe et al. (2016) using a first-order autoregression model with the autocorrelation coefficient set to give a decorrelation time scale of 600 s, an approximate eddy-turnover time scale.

- Land surface and hydrology parameterization—All UM configurations (global, R25-Africa, and CP4-Africa) use the JULES land surface scheme (Best et al. 2011; Clark et al. 2011) to calculate fluxes of energy, water, and momentum into the atmosphere. Subgrid heterogeneity in the CP4-Africa formulation is represented through nine surface tiles: five plant functional types (PFTs, including broadleaf tree, needle leaf tree, shrub, and C_3 and C_4 grasses) and four nonvegetated surface types (urban, inland water, bare soil, and land ice) with the surface energy balance computed for each tile. CP4-Africa simulations use the default four soil layers with thicknesses of 0.1, 0.25, 0.65, and 1.0 m, giving a total depth of 3 m. The tiles share a common soil water reservoir, with the Van Genuchten relationship (Van Genuchten 1980) used to calculate unsaturated soil hydraulic conductivity from soil moisture.

As far as possible, the model settings affecting the hydrological response of the land surface were therefore made consistent with those of the driving global model. The main exception to this is the choice of subgrid hydrology model. The CP4-Africa and R25-Africa configurations use the UKV surface hydrology scheme, that is, the Probability Distributed Model (PDM; Moore 1985) rather than a topography-based hydrological model (TOPMODEL; Beven and Kirby 1979), which is used in global configurations. There are uncertainties associated with both options, including consistency of the PDM parameters with soil properties, and the sensitivity of the TOPMODEL topographic index to model resolution, with implications for initializing the depth-to-water table, which can take decades to spin up. Although TOPMODEL has an advantage that is based on elevation data and may more accurately represent the presence of wetlands, it also introduces a longer soil moisture memory through the addition of a depth-to-water table that can impact on soil evaporation when the water table is within the active soil layer (top 3 m). In contrast the PDM does not have the same requirement and therefore any adjustments in the surface water

balance in response to a new hydrological regime will adjust relatively quickly a consideration also in the future climate simulations. Ideally, calibration of the PDM parameters would be carried out comparing routed runoff against observations of river discharge; however, for the purposes of this experiment the default JULES–PDM parameters are used.

The snow-free shortwave albedos are calculated using the spectral albedo model with scaling of near-infrared and visible albedos to observed values obtained from the GlobAlbedo dataset (Lewis et al. 2012).

c. Surface forcing

1) LAND–SEA MASK AND SURFACE TERRAIN

Regional model land–sea masks were created from the International Geosphere and Biosphere Programme (IGBP) land classification dataset. The IGBP dataset has a resolution of 30 arc s (on the order of 1 km) globally. The surface orography for the models is created from the Global Land One-kilometer Base Elevation (GLOBE) dataset (Hastings et al. 1999) using methods given in Webster et al. (2003). See section b in appendix A for details of a minor modification applied to the surface orography in the region around Mount Cameroon early in the simulation.

2) SOIL PROPERTIES

One of the key objectives of the CP4-Africa simulations is to determine the effects on the behavior of precipitation of explicit representation of convection. Previous convection-permitting simulations over West Africa (Taylor et al. 2013) have highlighted the sensitivity of convective initiation to mesoscale heterogeneity in land-surface properties. These simulations were able to reproduce observed sensitivities of convective initiation to soil moisture anomalies, resulting from antecedent rainfall. Standard configurations of the UM derive soil property information from the Harmonized World Soil Database (Walters et al. 2017a), which is considered to contain unrealistic small-scale variability across Africa (De Kauwe et al. 2013). To avoid contamination of the rainfall behavior, which might otherwise mask the realistic physical response to precursor precipitation, the soil properties in CP4-Africa were instead defined to be spatially uniform (and those of sand) across the whole domain. To allow a clean comparison with parameterized convection results, this was also applied to R25-Africa.

3) VEGETATION COVER

Land cover fractions for CP4-Africa and R25-Africa are derived from version 1.3 of the European Space Agency Climate Change Initiative (CCI) land cover dataset (CCI-LC; Poulter et al. 2015) for the epoch from 1998 to 2002. This is an important change from the standard IGBP-derived land cover mapping that is widely used (e.g., in the Cascade and IGBP land configurations) to provide subgrid land cover heterogeneity over nine tiles. This new high-resolution dataset improves the mapping from biome to PFT to provide a more realistic distribution of broadleaf trees in the Sahel and south of the Congo basin and higher bare soil fractions in comparison to IGBP in the northern fringes of the Sahel and a shift from C_3 to C_4 grasses, particularly in southern Africa (Fig. 2). The grid-box vegetation-type fractions are static in time and represent the maximum seasonal extent of vegetation.

The leaf area index is updated every five days using a monthly climatology created from MODIS collection 5 mapped to the five plant types used in the land surface nine-tile scheme.

4) SEA AND LAKE SURFACE TEMPERATURES

All the models (see Table 2) are forced with SSTs derived from the Reynolds dataset of daily high-resolution blended analyzes for SST (Reynolds et al. 2007). These data have a spatial grid resolution of 0.25° and are interpolated onto the regional model grids using bilinear interpolation.

Additionally, the model's land–sea mask contains numerous lakes, represented as inland sea points, which require input surface temperatures. The majority of these lakes are in eastern Africa, with the largest being Lake Victoria, covering 3502 grid boxes on the CP4-Africa grid. Where lakes are included in version 3 of the Along Track Scanning Radiometer (ATSR) Reprocessing for Climate (ARC) Lake Surface Water Temperature and Ice Cover (ARC-Lake) dataset (Hook et al. 2012; http://www.geos.ed.ac.uk/arclake/documents. html), a climatology from this dataset of monthly nighttime lake temperatures has been used. For other lakes (typically those with a surface area of less than $50 \, km^2$) a surface temperature value from the model's nearest sea point is assumed. The same approach was taken for the lakes in R25-Africa, while for the case of the global model, the Lake Victoria SSTs come from the GISST climatology (Rayner et al. 1996).

3. Experimental design

The lateral boundary conditions for both CP4-Africa and R25-Africa are supplied by a global model atmospheric simulation, which is a prototype version of the Global Atmosphere 7.0 (GA7) and Global Land 7.0 (GL7) configurations—the latest science configurations of the UM developed for use across all time scales. The
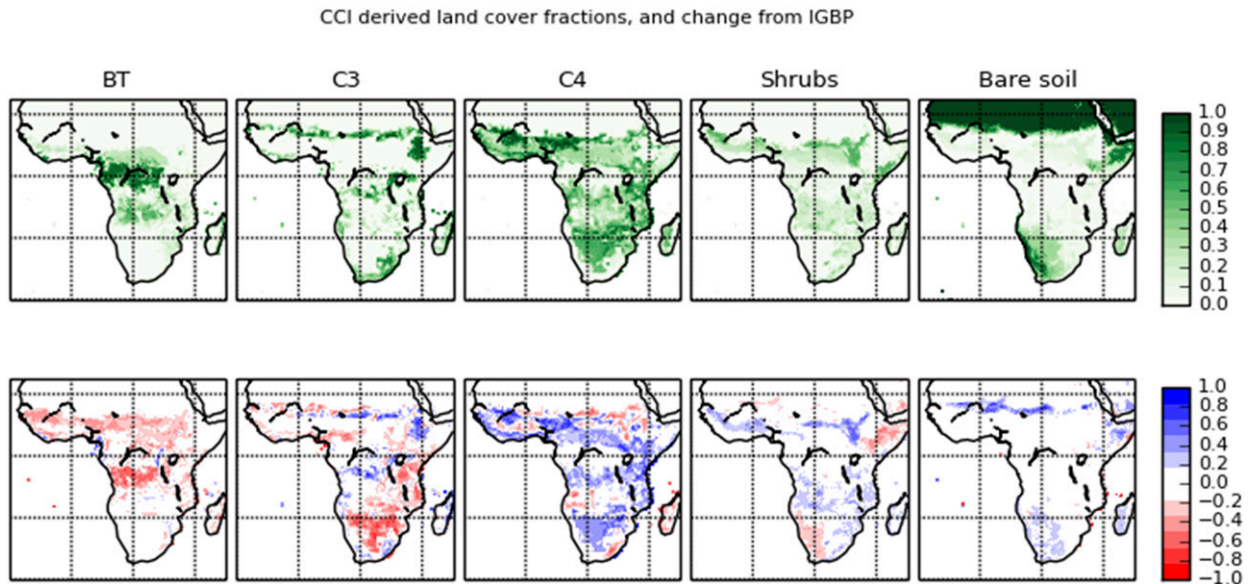
FIG. 2. (top) New CCI-derived land cover fractions for PFTs broadleaf trees (BT), C_3 and C_4 grasses, shrubs, and bare soil, and (bottom) the difference from the IGBP-derived fractions.

key differences between GA6/GL6 (Walters et al. 2017a) and GA7/GL7 (WGMD; Williams et al. 2017) are a new model aerosol scheme, a new snow scheme, revision to the parameterization of convection, plus a range of changes to the microphysics, cloud (Williams and Bodas-Salcedo 2017), and radiation.

The global simulation was run at N512 resolution (close to 26 km in the latitudinal direction by 39 km in the longitudinal direction over Africa), with 85 vertical levels (L85) and an upper boundary at 85 km. The atmospheric initial conditions for both the CP4-Africa and R25-Africa simulations are taken from global atmospheric model fields for 1 January 1997, following a 10-yr spinup period. The three-dimensional fields were interpolated onto the regional grids, taking account of the higher-resolution surface orography in the regional models. The exception to this is the soil moisture, the initialization of which is described below. The graupel prognostic (not present in the global model) was initialized to zero at the start of the run and, along with other convective-scale details, takes around 12 h to spin up in CP4-Africa.

a. Lateral boundary forcing

CP4-Africa and R25-Africa are forced by one-way nesting (Davies 2014) with lateral boundary conditions derived from the global atmospheric simulation. Three-hourly three-dimensional global model fields of the prognostic variables of winds, potential temperature, water vapor, cloud liquid water, cloud ice water, density, and Exner pressure are used to create these lateral boundary data. The 3-hourly data are linearly interpolated in time to the regional model time step.

b. Soil moisture initialization

The soil moisture fields for both CP4-Africa and R25-Africa were initialized with climatological data derived from an offline JULES land surface simulation on a 0.5° grid using the same sandy soil properties as were used in the CP4-Africa and R25-Africa simulations. This was forced with a bias-corrected reanalysis dataset: the Water and Global Change (WATCH) Forcing Data 2013 applied to ERA-Interim (WFDEI; Weedon et al. 2014), in which the monthly air temperature and rainfall totals are bias corrected against GPCC and CRU Time Series 3.1 (TS3.1) gridded observations. Initializing the soil moisture in this way is relatively fast and has the advantage of ensuring the soil moisture in all four soil layers is adequately spun up. The monthly mean soil moisture was computed based on the forcing period 2000–09 and the 0.5° climatologies were then downscaled using the climate data operators bilinear remapping tool (http://code.mpimet.mpg.de/projects/cdo) to produce the soil moisture fields at the required model resolution. Model instability problems during the early part of the simulation inadvertently led to an issue with soil moisture (see section c in appendix A).

c. Ozone, aerosols, dust, and greenhouse gases

The radiation and cloud microphysics schemes require three-dimensional fields of ozone mixing ratio, aerosols, and dust particles. Climatological values are

assumed for all, and these are updated in the model every five days. Ozone fields are obtained from climatological monthly means for the period 1994–2005, generated from Stratosphere–Troposphere Processes and Their Role in Climate (SPARC-II) ozone data (Cionni et al. 2011). The data for the various aerosols species and dust are derived from 20-yr climatological monthly means from a GA6/GL6 Walters et al. (2017a) AMIP simulation from 1989 to 2008 with the Coupled Large-Scale Aerosol Simulator for Studies in Climate (CLASSIC) interactive aerosols and dust scheme (Bellouin et al. 2011). The climatological aerosols included in these simulations are organic carbon, black carbon, biogenic aerosol, sulfate aerosol, biomass burning aerosols, and six different sizes of dust.

Various greenhouse gases are assumed to have fixed global values, which are varied annually over the 10-yr simulation. Carbon dioxide mass mixing ratios are varied from $5.516\,79 \times 10^{-4}\,\mathrm{kg\,kg}^{-1}$ for 1997 to $5.814\,88 \times 10^{-4}\,\mathrm{kg\,kg}^{-1}$ for 2006 in the same way as in the global model. The other gases with fixed global annual values are methane, nitrous dioxide, dichlorodifluoromethane (CFC12) and tetrafluoroethane (HFC134a).

d. Length of the experiments and their evaluation

The CP4-Africa simulation has run for just over 5 years at the time of writing, and will be continued to 10 years in total. The 10-yr R25-Africa control simulation has been completed. Idealized future climate simulations representing a period of 10 yr around 2080–2100 are now starting with both models and will be the focus of subsequent papers. Partners in the FCFA program will be analyzing both control and future climate simulations in great detail comparing against all available observations over Africa together with satellite and reanalysis climatologies in a number of future studies. This paper presents results from a first initial analysis against a limited number of widely used observational precipitation climatologies: GPCP (Adler et al. 2003), TRMM (Kummerow et al. 1998; Huffman et al. 2007, 2010), CMORPH (Joyce et al. 2004), the HadCRUT3 (Brohan et al. 2006) near-surface temperature climatology, and the CERES (Loeb et al. 2009) top-of-the-atmosphere (TOA) outgoing shortwave radiation climatology.

Africa is a region with a sparse network of observing stations, with few countries having long-term high quality, high-density station observations. This makes it difficult to validate climate models over Africa. Much of the evaluation of climate models precipitation over Africa relies on using satellite climatologies. TRMM and CMORPH are derived from a combination of infrared and microwave sounders, and their results have been calibrated against gauge data. GPCP is a combined satellite–gauge product. It shows better consistency with gauge-based precipitation products (Nikulin et al. 2012), but provides data at a coarser temporal (daily as opposed to 3 hourly) and spatial (1° compared to 0.25°) resolution than TRMM and CMORPH. Satellite precipitation data have been assessed against surface observations in regions of the globe with high quality high-density surface observations (e.g., Europe; Prein and Gobiet 2017), but even over Europe there is uncertainty particularly in regions of mountainous terrain. Over Africa, TRMM and CMORPH have been found to have quite different characteristics in terms of day-to-day variability (Martin et al. 2017), which is likely related to the different satellite data sources and algorithms used in each case. It is known that both datasets tend to underestimate smaller daily rainfall totals and can overestimate larger ones (e.g., Tian et al. 2010). TRMM rainfall is somewhat more intermittent than CMORPH, and Xie et al. (2017) conclude that CMORPH, version 1.0, is better than TRMM at 3-h and daily time scales. On seasonal time scales, TRMM (version 6) tends to have less precipitation than GCPC over Africa (Nikulin et al. 2012). The large difference between TRMM and GPCP is explained by the fact that both products are adjusted to large-scale monthly precipitation from gauge networks but use different gauge analysis products, with GPCP using a more recent version than TRMM (version 6).

4. Model sensitivity studies

The CP4-Africa model configuration uses some settings not widely tested prior to this simulation. Short sensitivity tests were run to test the new options, which include corrections to moisture fields to enforce the conservation of moisture (section 4a) and the inclusion of boundary layer stochastic perturbations (section 4b).

a. Enforcing conservation of moisture in the regional model

Unlike flux-formulated schemes, semi-Lagrangian advection schemes are typically not designed to locally conserve the advected quantities. Correctors can be applied but most methods rely on a calculation of global error (e.g., the change in the domain-integrated quantity that arises from advection), which is then used to apply a correction to improve, rather than guarantee, local conservation. Such a scheme is applied in the global UM, but in regional configurations the issue is complicated by the need to account for fluxes through the lateral boundaries in the calculation of the error. Aranami et al. (2015) have developed a scheme that accounts for these boundary fluxes and this has been implemented in
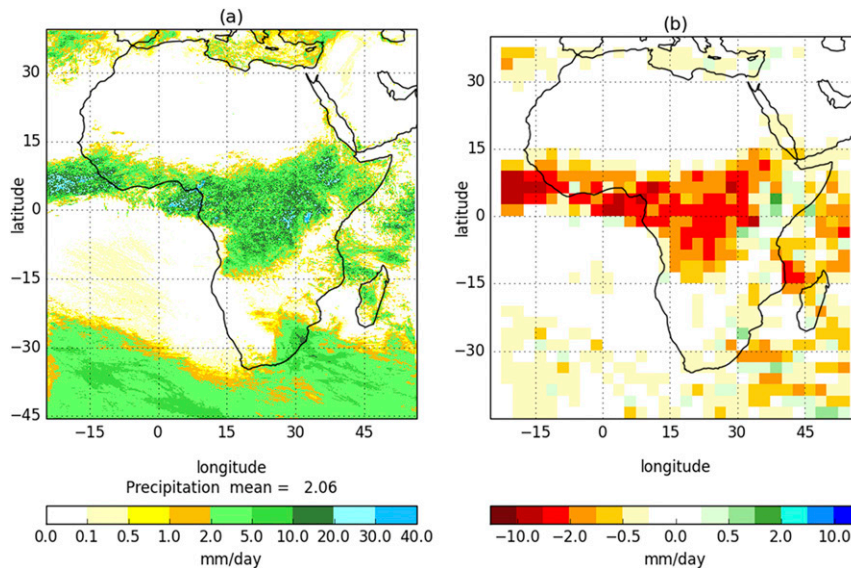
FIG. 3. Mean precipitation for the 29 days of October 1988 from the CP4-Africa simulations for (a) with conservation and (b) with conservation minus control. The data have been regridded to give a less noisy difference plot.

CP4-Africa to ensure conservation of the total amount of all moisture variables and reduce local conservation errors. Unfortunately, attempts to use the new scheme in a model without graupel and with convective parameterization failed, so R25-Africa has no moisture conservation being applied (see Table 2).

The impact of switching on the Aranami et al. (2015) scheme was assessed using two 29-day-long simulations for October 1988 with and without the scheme. Figure 3 shows the mean precipitation with conservation together with the difference between the runs. The effect of moisture conservation is to reduce the mean precipitation for the whole region from 2.54 to 2.06 mm day^{-1}. This is closer to the GPCP (Adler et al. 2003) climatologically observed value of 1.65 mm day^{-1} but suggests that the model precipitation rate may still be too high even when conservation is enforced, as it is outside the interannual standard deviation of 0.19 mm day^{-1}. Based on this one month, it appears that conservation has little impact on the spatial pattern of mean precipitation and, rather, tends to reduce the mean values everywhere.

While the conservation scheme has reduced the monthly mean precipitation everywhere, the more significant impact is on shorter time scales and the rainfall extremes. As shown in Fig. 4, the distribution of hourly precipitation rates is affected by the conservation. The frequency of very high unrealistic rates, greater than 4000 mm day^{-1}, in the control simulation are greatly reduced by the conservation scheme, suggesting that these were spurious, resulting from transport errors in the model, which presumably acted to either directly increase

the local water content, which then led directly to an increase in precipitation, or perhaps intensified convection as a source of spurious latent heating. Since extreme rainfall is an important consideration within the IMPALA project, the inclusion of moisture conservation is clearly an important improvement to the model formulation.

b. Boundary layer stochastic perturbations

The impact of adding the boundary layer stochastic perturbations described in section 2b was assessed during a 30-day run for January 1997. The control in this
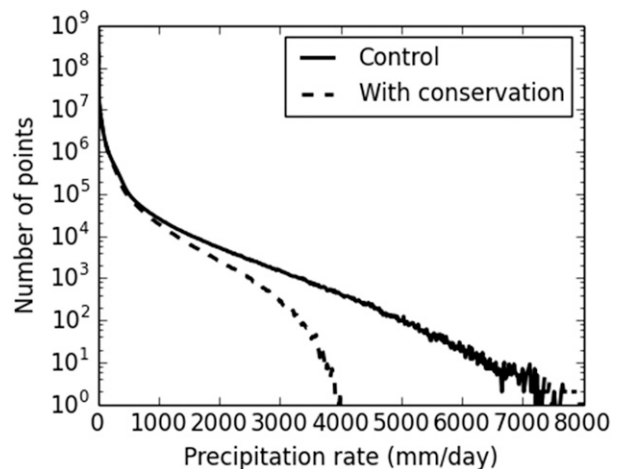

FIG. 4. Distribution of hourly mean precipitation rates from the 29 days of the October simulations. The *y*-axis scale refers to the number of grid points.

case includes the moisture conservation scheme (section 4a). The stochastic perturbations have negligible impact on the mean January precipitation for Africa, increasing it slightly from 2.07 to 2.09 mm day^{-1} compared with a GPCP January climatology of 1.9 mm day^{-1}. The impact of the perturbations on the diurnal cycle of precipitation has been examined within different regions of Africa (not shown). The perturbations cause a slight increase in the amplitude of the diurnal cycle over the sea to the west of Africa, but do not affect the phase. Over land the perturbations result in an earlier onset of precipitation, presumably because they facilitate the growth of explicitly resolved eddies that grow into convective clouds. A 1-month-long sensitivity test is too short a period to compare with observations and draw any reliable conclusions.

5. Results

The results presented in this paper are based on the initial five years' worth of the CP4-Africa simulation. A wide selection of fields are output on hourly, 3-hourly, 6-hourly, and daily time scales for the whole of the regional grid and will be the subject of detailed analysis in subsequent papers. Here, results from the period June–August (JJA) will be used to make an initial assessment of the performance of CP4-Africa compared to R25-Africa, the driving global model, and available long-term climatologies. JJA was chosen on the basis that our global model has a long-standing dry bias over West Africa during the summer monsoon period (Walters et al. 2017a, their Fig. 16).

a. Analysis of JJA seasonal means

CP4-Africa has more precipitation over western and eastern Africa (Figs. 5a,b) than either the global model or R25-Africa, substantially reducing the dry biases seen in the coarser-resolution models. Along the edges of the Sahara the precipitation in CP4-Africa extends slightly farther north, again better matching the observations. On its native grid (Fig. 5a), CP4-Africa precipitation contains finescale (sub-R25-Africa grid) detail with high values over the steep mountains in central West Africa, leading to a wet difference relative to GPCP. The precipitation over the ocean along the ITCZ to the west of Africa is also higher relative to GPCP whereas the dry bias in the coarser-resolution models extends out over the ocean. Over South Africa CP4-Africa has less precipitation, which is confined to the east coast in better agreement with climatology than the coarser-resolution models. Over the Atlantic Ocean, in the southwestern part of the domain, all three models have excessive precipitation, the bias being unaffected by the use of a convection-permitting model.

Biases in the R25-Africa and global simulations are very similar (Figs. 5c,d), suggesting that differences in the model land surface scheme and soil type have little impact on simulated seasonal mean rainfall.

Consistent with the reduced precipitation biases over the Sahel and along the ITCZ in CP4-Africa, there are also substantial increases in the outgoing shortwave radiation across western, central, and eastern Africa north of the equator (Fig. 6). This is a region of deep convective activity, which suggests that the 4.5-km simulations have brighter deep convective cores, in better agreement with CERES (Loeb et al. 2009). Convection-permitting simulations of the order of 4 km are known to have problems simulating convective anvil tops (Bryan and Morrison 2012; Stein et al. 2015) Over land, between 5°S and 15°N the bias changes from significantly too little outgoing shortwave flux in the R25-Africa and global model to slightly too much at 4.5 km, notably in the south of the region. South of the equator over land there is a general small positive bias in the CP4-Africa outgoing shortwave radiation. In the stratocumulus region off the coast of Namibia, the CP4-Africa simulation has an enhanced positive shortwave radiation bias compared to the R25-Africa and global model, likely associated with brighter clouds.

Generally the outgoing shortwave radiation biases for the R25-Africa and global simulations are similar, but there is a marked difference over the Namibian coast stratocumulus region. The clouds in this region are slightly different in the two models with a smaller cloud water bias in the global simulations than in R25-Africa (not shown). Both models use the same microphysics parameterization but the global model includes prognostic aerosol rather than using climatology. It seems likely that this will result in differences in cloud liquid water. It is also possible that the amount of biomass-burning aerosols over the bright stratocumulus may be different, altering the absorption of radiation and leading to lower values in the global simulation.

A comparison of the JJA 5-yr seasonal means of the daily maximum and minimum near-surface temperatures with HadCRUT3 (Brohan et al. 2006) shows substantial differences in the CP4-Africa simulations compared to R25-Africa and global model (Figs. 7 and 8). Both maximum and minimum temperatures are lower than the other models over the whole of Africa, resulting in a cold bias relative to HadCRUT3 for maximum temperatures over most of Africa and a reduced warm bias for minimum temperatures over central and southern Africa. The overall biases in CP4-Africa, although different in sign, are typically smaller or of the same size as the other models. The largest cooling in CP4-Africa relative to
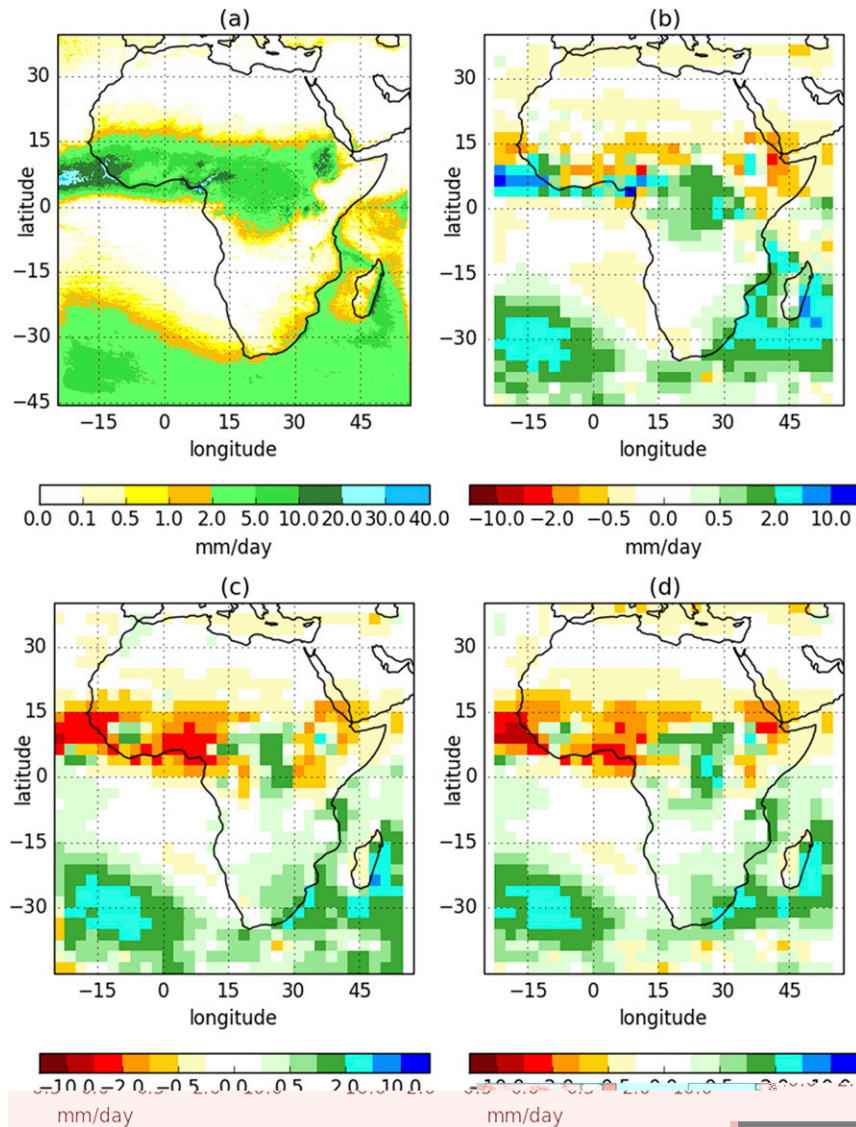
FIG. 5. JJA seasonal mean precipitation for 1997–2001 from (a) CP4-Africa on its native grid, (b) CP4-Africa minus GPCP JJA climatology for 1979–98, (c) R25-Africa minus GPCP climatology, and (d) the driving global model minus the GPCP climatology. In (b)–(d), the model data have been regridded onto the GPCP grid.

R25-Africa is seen in the regions of convection (i.e., where there is high precipitation over land in Fig. 5a). This cooling is due to the presence of more bright cloud reflecting the incoming shortwave radiation (Fig. 6) and hence reducing heating at the surface. Over non-convecting regions, changes may be due to several factors: changes in nonconvective cloud resulting from a different cloud scheme, changes in clouds and their overlap resulting from more vertical levels, and changes in the boundary layer behavior during the day and night resulting from a convection-permitting model. R25-Africa and the global model have fairly similar differences from

HadCRUT3 for the daily maximum apart from over central Africa (5°N–15°S), where the global model is cooler. This difference may be related to the difference in the representation of aerosols and is less obvious in the daily minimum temperature. Note that as station data over parts of Africa are scarce, better agreement with HadCRUT3 does not always provide a clear indication that the model is better.

b. Variability

In general, global models with a convection parameterization have thus far provided a poor simulation of the
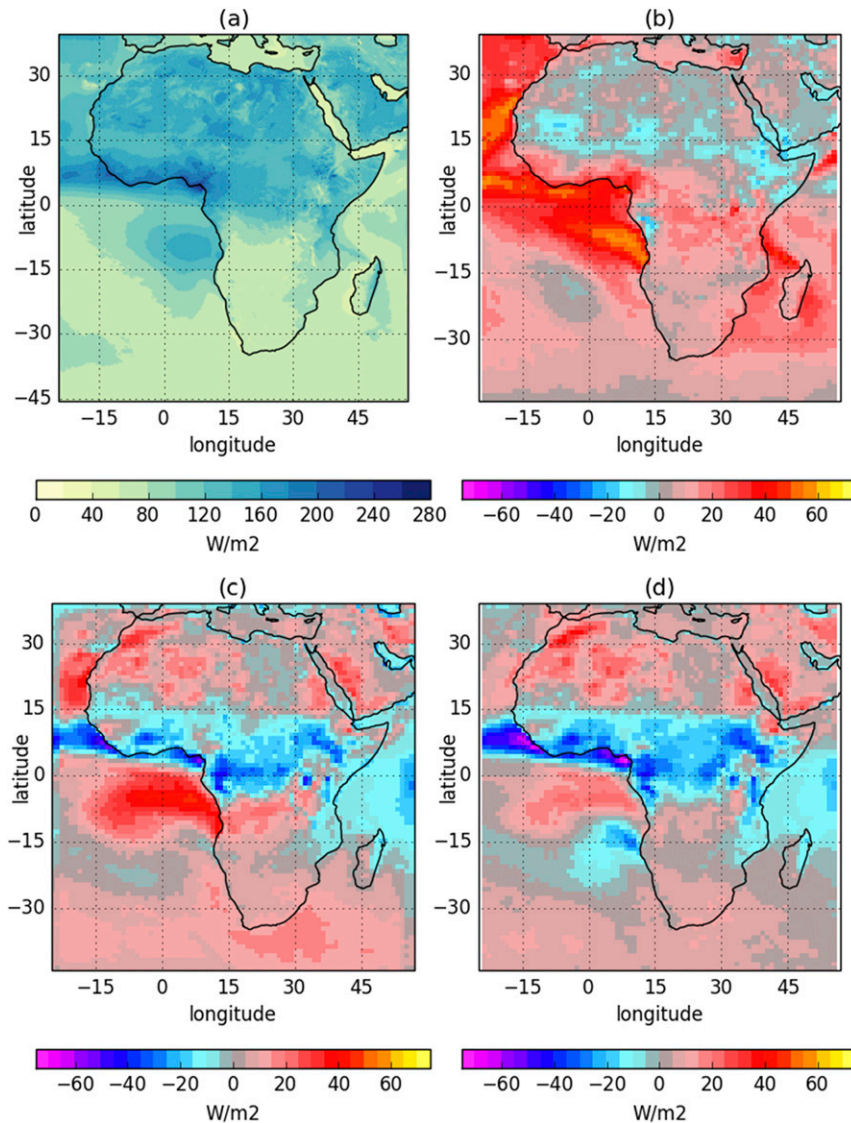
FIG. 6. JJA outgoing shortwave radiation (W m^{-2}) for 1997–2001 from (a) CP4-Africa on its native grid, (b) CP4-Africa minus CERES JJA climatology for 2000–13, (c) R25-Africa minus CERES, and (d) the driving global model minus CERES. In (b)–(d), the model data have been regridded onto the CERES grid.

movement of rain-bearing systems such as westward-propagating mesoscale convective systems embedded within African easterly waves (Bain et al. 2011). Observations such as TRMM 3B42 rainfall show how these are coupled to the convective precipitation (see Fig. 9c for a latitude band 5°–15°N during June 1998). Comparing Figs. 9a and 9c shows that the CP4-Africa simulation contains a realistic signal of systems moving westward at the correct speed and with only a few moving eastward, in good agreement with the TRMM observations. R25-Africa captures some westward movement of precipitation over several days (Fig. 9b) but also contains

eastward-moving systems during the day and a very strong diurnal cycle over the whole of the African continent (Fig. 9b). There remains a diurnal signal in CP4-Africa too, which is somewhat stronger than in TRMM but much weaker than that of R25-Africa and with more day-to-day variability.

Examination of the distribution of daily rainfall intensity across the West African monsoon (WAM) region (Fig. 1) reveals that CP4-Africa produces more precipitation than R25-Africa overall, with substantially more at higher rain rates (Fig. 10). This compares well with observational data from TRMM and CMORPH, and is a significant
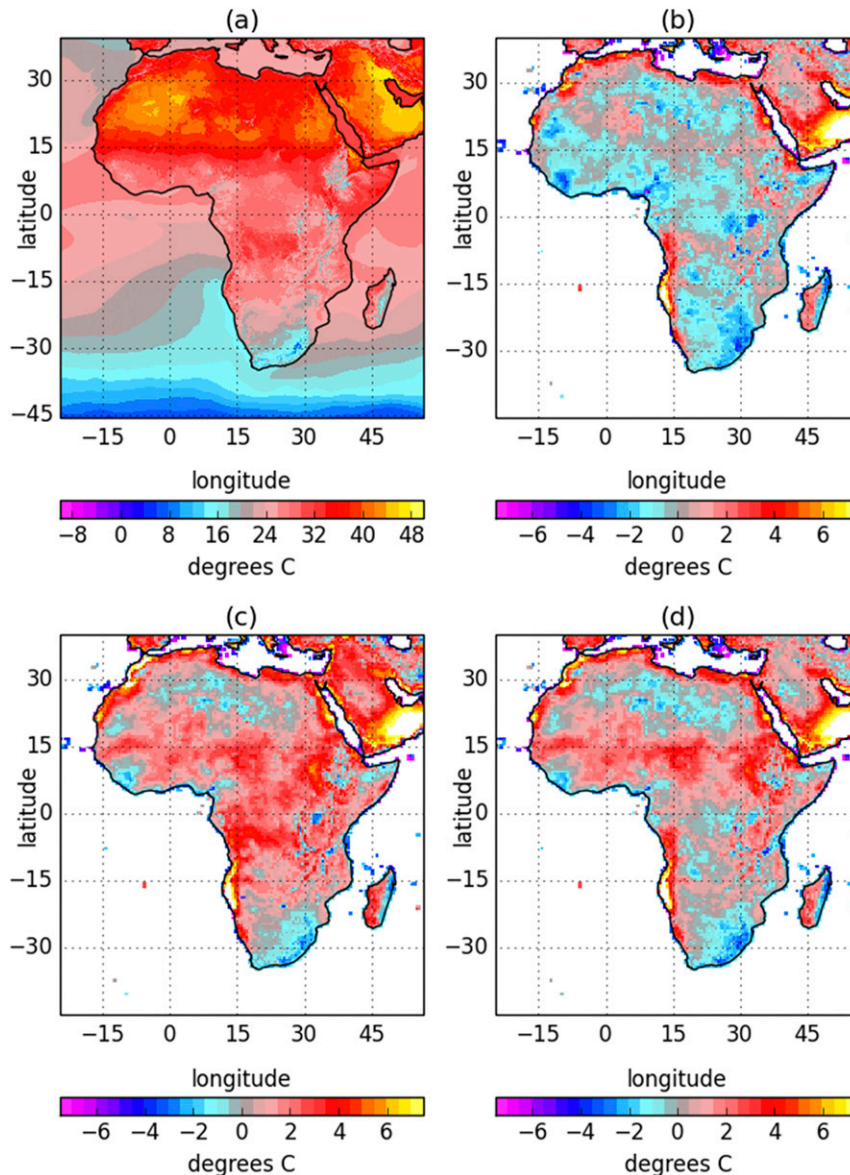
FIG. 7. JJA mean daily maximum 1.5-m temperature (°C) for 1997–2001 from (a) CP4-Africa on its native grid, (b) CP4-Africa minus HadCRUT3 JJA climatology for 1979–98, (c) R25-Africa minus HadCRUT3, and (d) the driving global model minus HadCRUT3. In (b)–(d), the model data have been regridded onto the HadCRUT3 grid.

improvement over the results with parameterized convection (R25-Africa). The model still lacks the high 3-hourly precipitation events [$>100\,\mathrm{mm\,day}^{-1}$, on the order of $12.5\,\mathrm{mm}\,(3\,\mathrm{h})^{-1}$] when coarse grained to low resolution (3° latitude × 3.75° longitude). This is in contrast to the very high hourly precipitation rates observed on the model's native grid when looking at daily mean precipitation (not shown). R25-Africa produces less rainfall overall than either the observations or CP4-Africa and this arises from too many weak precipitation events ($<7\,\mathrm{mm\,day}^{-1}$) and a substantial underestimation

of moderate and high precipitation events. Both models have too many events with precipitation rates between 10 and $20\,\mathrm{mm\,day}^{-1}$ relative to the observations.

Kendon et al. (2014) have shown the importance of explicitly resolved convection on the spatiotemporal distribution of rainfall for a regional simulation over the United Kingdom. Here, we repeat their analysis for the WAM region and regrid the models to the TRMM data resolution (0.25°) for comparison (Fig. 11). The TRMM probability distribution shows a large number of short-duration events of higher intensities, above $0.5\,\mathrm{mm\,h}^{-1}$.
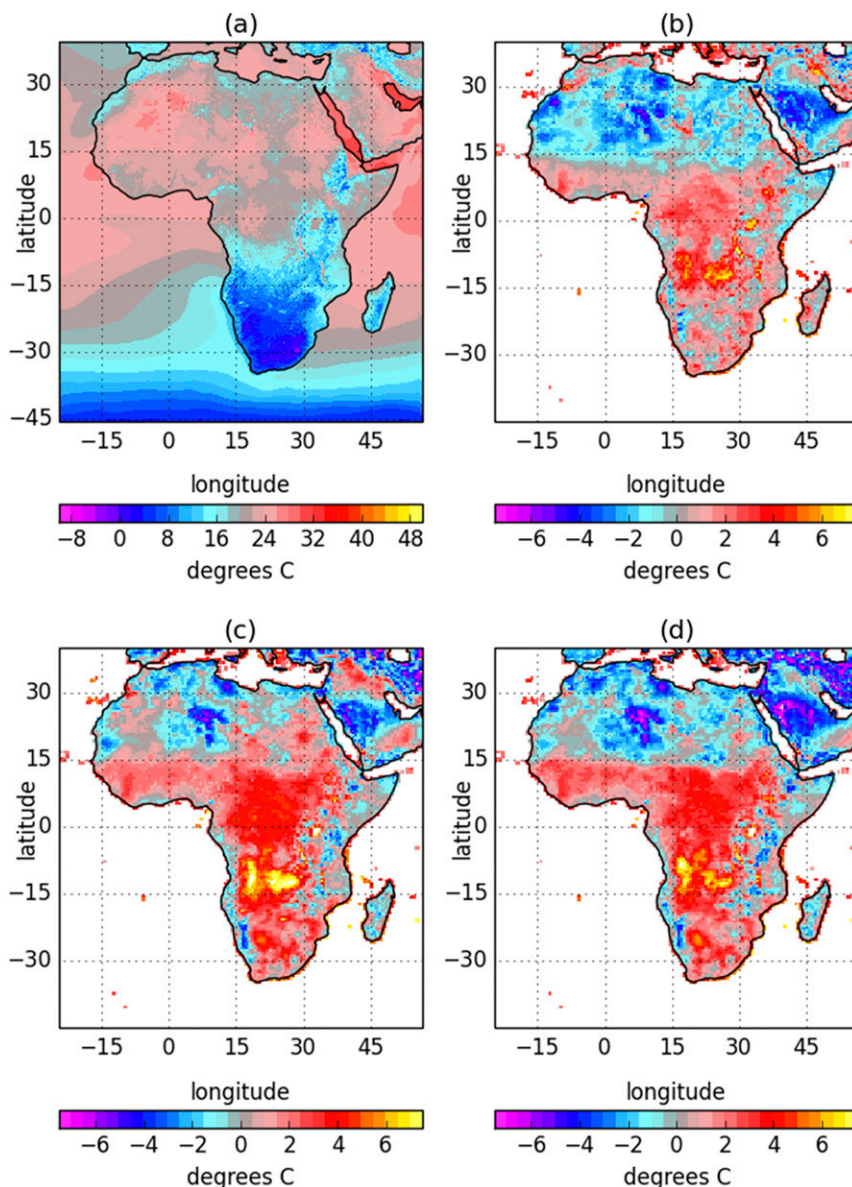
FIG. 8. As in Fig. 7, but for mean daily minimum 1.5-m temperature.

The CP4-Africa simulation provides substantially more short-duration, high-intensity events than R25-Africa and fewer low-intensity events lasting over 3 h, in better agreement with the observations. R25-Africa has a large number of precipitation events with 0.2–1 mm h^{-1} lasting between 6 and 9 h and very few higher-intensity events. These findings are qualitatively similar to those of Kendon et al. (2014), although analysis of a longer dataset would be required to assess the significance of the results.

c. Diurnal cycle of convection

In all regions (Fig. 1, regions A–F) the diurnal cycle of CP4-Africa is improved relative to R25-Africa and

the global model with a later peak in rainfall, although this is still too early relative to TRMM for most regions (Fig. 12). In western and central Africa (Figs. 12a,b) the mean CP4-Africa precipitation agrees well with TRMM overnight, but peaks about 3 h too early and is too high during the day in western Africa. R25-Africa and the global model produce less precipitation and also peak 3 h or more too early but with a secondary peak in precipitation at around 2100 UTC, which is not present in TRMM. In the west and farther north (Figs. 12e,f), the magnitude of the CP4-Africa precipitation agrees better with the TRMM observations throughout the day, but still peaks up to 2 h too early.
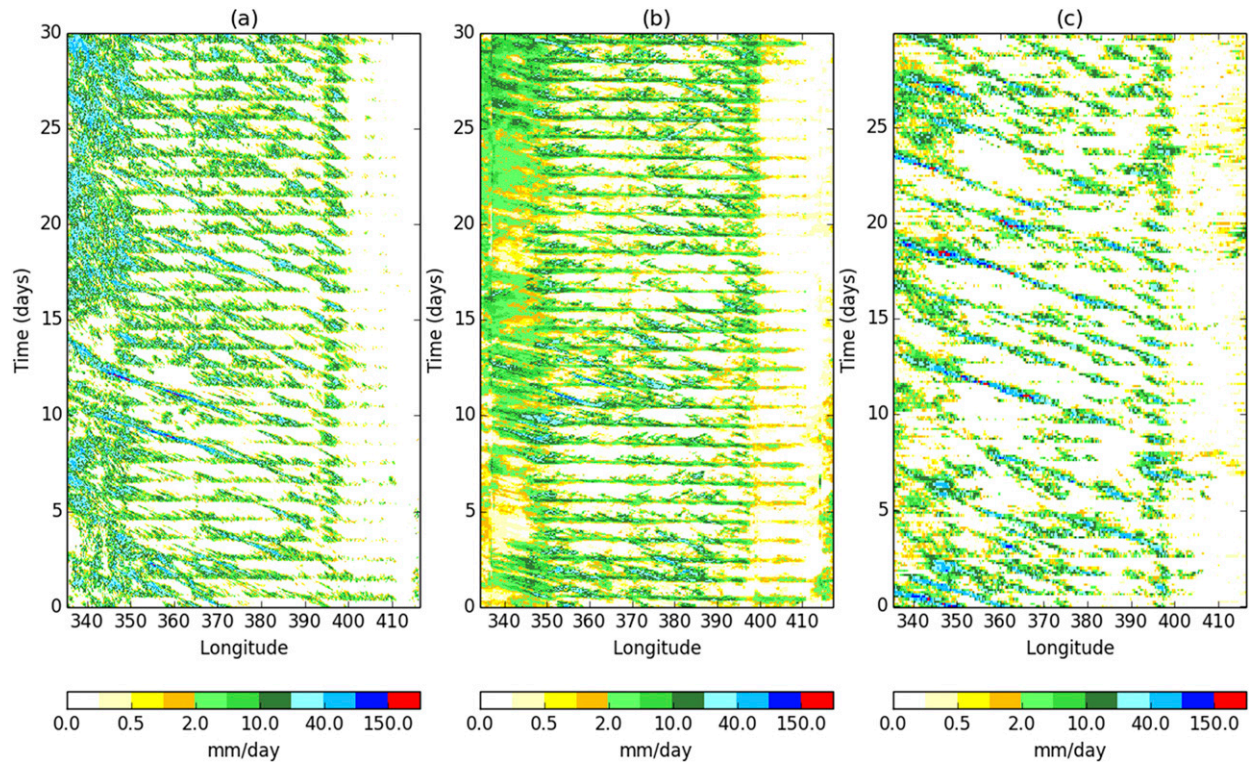
FIG. 9. Hovmöller plots of hourly mean precipitation for the latitude band 5°–15°N for June 1998. Time (days) increases along the *y* axis. Results are shown for (a) CP4-Africa, (b) R25-Africa, and (c) 3-hourly TRMM data.

R25-Africa and the global model have an earlier peak and show little correlation with TRMM, lacking precipitation overnight. In the east, (Fig. 12b) the amplitude of the diurnal cycle is too strong in all the models relative to TRMM. The timing of the peak in CP4-Africa is in better agreement with TRMM but there is too much precipitation overnight, which persists into the early morning. This suggests that perhaps CP4-Africa contains too many large organized convective systems overnight in this area. Farther south (Fig. 12d), the CP4-Africa diurnal amplitude is more than double that of TRMM but with a peak at approximately the correct time of day.

Figure 13 shows the mean diurnal variation in the number and size of buoyant cloudy updrafts at a height close to 6 km for the regions A–F shown in Fig. 1. A height of 6 km was chosen because this lies above the freezing level for Africa, and so the plumes reaching this height will be associated with deep convection. Buoyant cloudy updrafts were calculated from hourly model output averaged over 30 × 30 grid points (i.e., to a 135-km grid on a set of fixed heights). For each coarse-grid area and height, buoyant points are those with cloud water or ice present and upward vertical velocity (>0), and that are buoyant relative to the coarse grid. Distinct plumes are identified by checks against neighboring points and the mean size calculated. The algorithm ignores the fact that buoyant points along the edges of the 30 × 30 points may be part of a bigger plume in the neighboring coarse 135-km regions but it provides a first indication of typical size of the plumes to differentiate isolated deep convection from mesoscale convective systems. Figure 13a shows that the number of plumes is a minimum between 0800 and 1200 UTC and a maximum between 1500 and 1800 UTC, both corresponding to the minimum and maximum in the diurnal cycle of precipitation (Fig. 12). The variation in the size of the plumes tends to lag the cycle in the number of plumes. As the evening progresses, the number of plumes decreases but their size tends to increase, peaking around midnight, suggesting the convection is becoming more organized. While buoyant plumes are not directly measurable, their area is an indicator of the strength and size of the convection and will be linked to observable quantities like OLR and cloud. Studies of the size of convective systems over West Africa based on measurements of OLR (Pearson et al. 2010) and of the life cycles of deep convection over the whole of Africa using TRMM and geostationary satellite data (Futyan and Del Genio 2007;
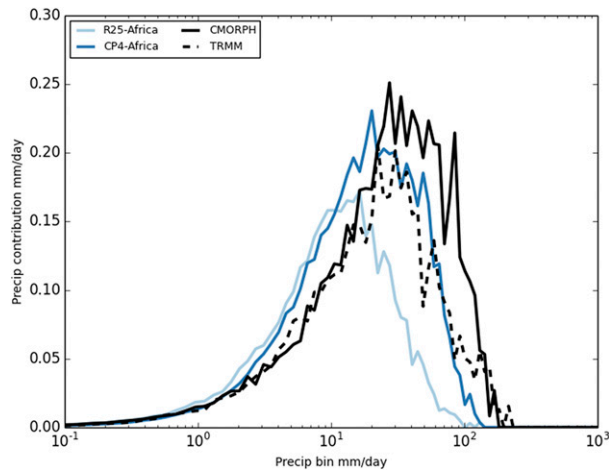
FIG. 10. Contribution of different 3-hourly precipitation events (mm day^{-1}) to the average 3-hourly precipitation rate for the WAM region (Fig. 1) for June–September (JJAS) 1997. CP4-Africa and R25-Africa results are shown along with two observational datasets: CMORPH (Joyce et al. 2004) and TRMM 3B42 version 7A (Kummerow et al. 1998; Huffman et al. 2007, 2010) . All data were first regridded onto a common coarser resolution of N48 (3° latitude × 3.75° longitude; Klingaman et al. 2017) to aid comparison.

Laing and Fritsch 1993) find that convection starts off during the early afternoon as smaller isolated deep clouds and becomes more organized later in the evening and through the night as larger mesoscale convective cloud systems. Figure 13 illustrates how information that cannot be directly observed but that may be important to improving parameterization of convection can be estimated from the CP4-Africa simulation.

6. Summary

In this paper we have documented the experimental design and initial results from the first experiment with the Pan-African Convection-Permitting Regional Climate Simulation with the Met Office Unified Model (CP4-Africa). This has been run under the IMPALA project within the Future Climate for Africa program and is designed to deliver a better understanding of the roles played by improved local representation of convective processes and high-impact weather on the climate variability and change over the continent and is to be used to improve convective and land–atmosphere coupling in the coarser-scale models.

An important advance on earlier regional UM convection-permitting simulations is the inclusion of changes to ensure moisture conservation. This

reduces the occurrence of unrealistically high grid-box precipitation rates, giving closer agreement to the observations. The CP4-Africa experiment is driven directly from a global 25-km, 10-yr AMIP simulation for the years 1997–2006. To date, the simulation has completed a 5-yr run. An additional R25-Africa regional simulation with parameterized convection and driven with exactly the same lateral boundary forcing and soil properties as CP4-Africa has completed a 10-yr run and is an important step in aiding our understanding of the results for the following reasons:

- It can be used to look at the impact of changing the soil type, vegetation, and some aspects of the land surface scheme over Africa at coarse resolution by comparison with the global model.
- It can be used to assess whether the use of climatological aerosols is having an impact over Africa by comparison with the global model.
- It has the same high-frequency output (i.e., hourly or 3 hourly) as CP4-Africa, allowing for the study of the subdaily behavior of a convection-permitting model with a model with convective parameterization. The global model simulation has a reduced selection of output at lower frequency (3 hourly, 6 hourly, or daily).

The first results from the simulations indicate there is a substantial improvement in the CP4-Africa JJA average rainfall results over those of R25-Africa and the global model. This is true across most parts of the African continent with, most notably, a reduced dry bias over the Sahel and an associated reduction in radiative biases resulting from the presence of brighter, more organized convective clouds. Over the stratocumulus region to the west of Africa, particularly where cloud–aerosol interactions are important, both regional models perform rather worse than the global model, at least partly because of the simplified representation of aerosols in these models. Encouragingly, the initial results presented here suggest that the variability and spatiotemporal characteristics of the rainfall all appear to be better represented in CP4-Africa. There is evidence of westward-propagating convective systems and a better distribution of 3-hourly precipitation events compared with the observations. As expected from previous studies (Birch et al. 2014b), the diurnal cycle of convective precipitation over land is better handled in the CP4-Africa simulation, although there is still a tendency for rain to initiate too early in the day. The most extreme intense but short-lived rainfall events are also better captured, consistent
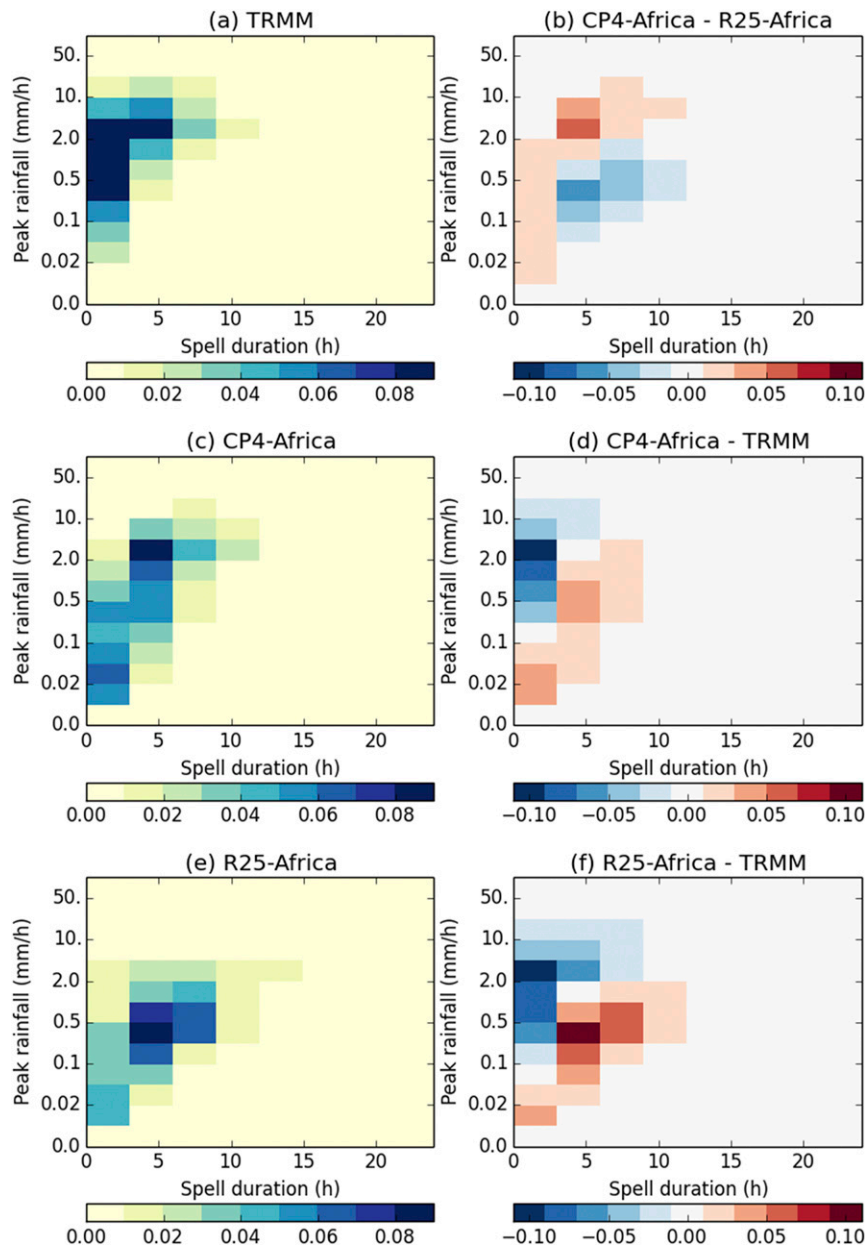
FIG. 11. Plots of the joint probability distribution of wet spell duration vs peak rainfall intensity for the WAM region (8°–17°N, 15°W–10°E; see Fig. 1) during JJA 1998–2001. Shown are the distribution for (a) TRMM, (c) CP4-Africa, and (e) R25-Africa and (b),(d),(f) the differences.

with results found over the United Kingdom (Kendon et al. 2014).

The control CP4-Africa simulation is expected to complete 10 years' worth of simulation toward the end of 2017 with the future-climate CP4-Africa run completing after this. The data are already available to all FCFA projects to aid in their analyses of the regional climate of Africa. The data from both simulations will be released to the general public when the FCFA projects are expected to be completed in July 2019. The encouraging first results presented here suggest that there are good reasons for optimism for greater confidence in future projections for Africa, both directly from the CP4-Africa simulations and also as our understanding of the processes from using this model leads to improving parameterizations in coarser-resolution models.
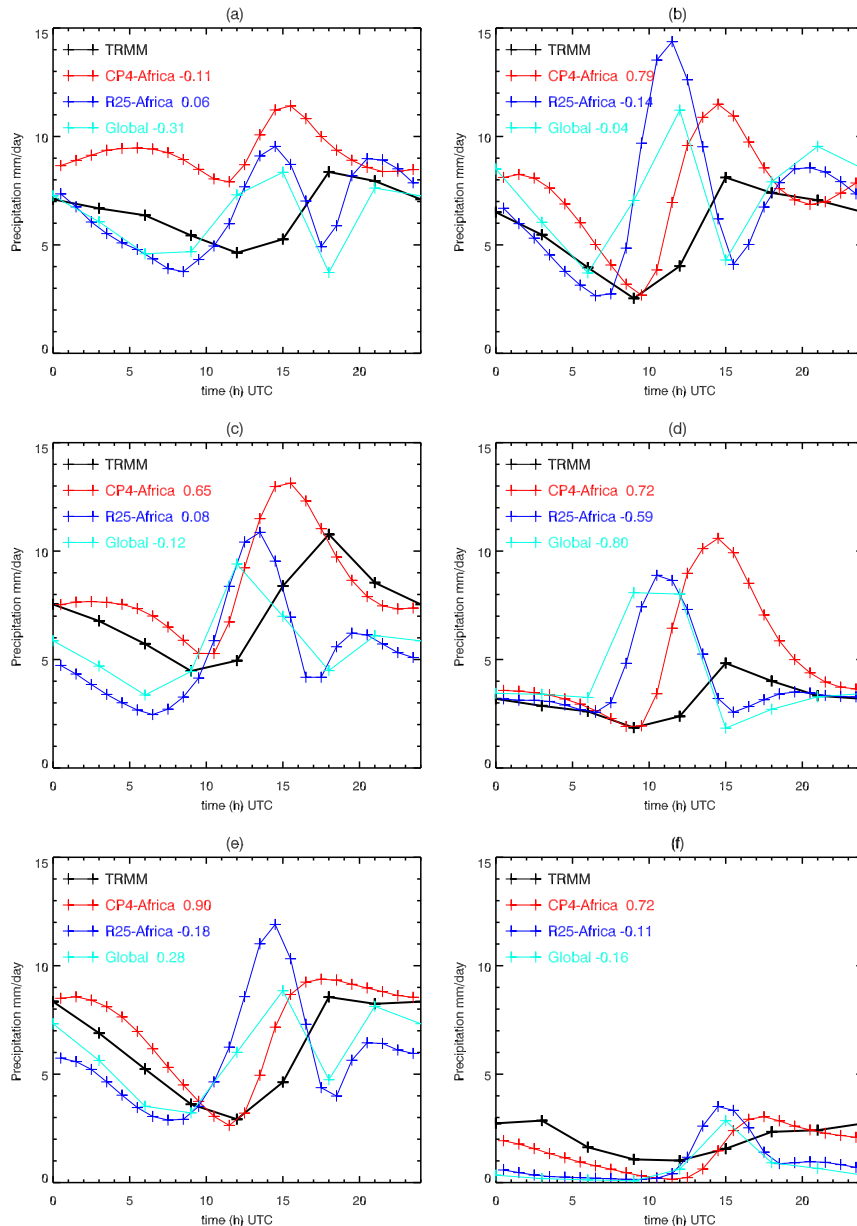
FIG. 12. The mean diurnal cycle of precipitation for JJA in the CP4-Africa, R25-Africa, and global simulations along with TRMM data for the six regions shown in Fig. 1: (a) A (5°–10°N, 0°–15°W), (b) B (5°–10°N, 15°–30°E), (c) C (5°–10°N, 0°–15°E), (d) D (5°S–5°N, 15°–30°E), (e) E (10°–15°N, 0°–15°W), and (f) F (15°–20°N, 0°–15°W). The regional model results are derived from hourly mean precipitation averaged over JJA. The global model means are derived from 3-hourly instantaneous precipitation rates. The numbers in the legend are the correlation coefficients between TRMM and the respective model values.
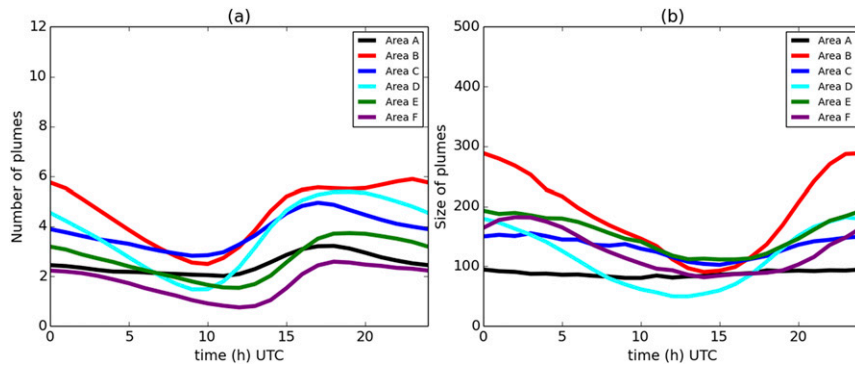
FIG. 13. The mean diurnal cycle of (a) the number of buoyant plumes and (b) the mean buoyant plume size (km^2) for regions A–F shown in Fig. 1.

APPENDIX A

Model Issues

a. Model time step

The CP4-Africa model time step was initially set to 100 s, but because of problems with stability in November 1999 of the simulation this was reduced to 75 s from 1 November 1999. The rerun referred to in section b of this appendix also used a 75-s time step.

b. Mount Cameroon

During July of the first year of the CP4-Africa simulation, a moist grid point storm occurred over Mount Cameroon, an isolated steep-sided mountain close to the coast of West Africa, which is a region of heavy convective precipitation during the summer months. This resulted in a model failure. Investigation revealed that this was associated with the ascent of warm moist air over the mountain, releasing latent heat and leading to excessive vertical velocities that resulted in numerical instability. Since it seemed likely that further similar failures would occur later in the simulation, a pragmatic choice was made at this point to perform some local smoothing of the orography, which was restricted to the immediate vicinity of Mount Cameroon only. Tests demonstrated that this was an effective strategy, and so the simulation was restarted on 1 July 1997 with this minor modification.

c. Soil moisture reset

Unfortunately, the reconfiguration of the model prognostic fields after six months outlined in the previous section of this appendix resulted in resetting the soil moisture fields everywhere to their saturated values. This "saturation" event went undetected until time series of soil moisture and runoff were examined after three years' worth of simulation. Of the additional 782 mm of water added (on average across the domain), 272 mm (35% of this water) is lost within the first five days, of which 254 mm is via subsurface runoff, which is then lost to the model. The impacts of the soil moisture reset on moisture fluxes to the atmosphere are summarized in the time series plots of evaporation (Fig. A1), that is, plant transpiration (Et) and bare soil evaporation (Es) and the deep-level (1–3 m) soil moisture for three cases: bare soil, deep rooted vegetation, and shallow rooted vegetation. For bare soil, moisture fluxes are via bare soil evaporation, which is derived from the top soil level only. The reservoir for bare soil evaporation is around 40 mm and so the impact of elevated moisture fluxes is short lived (~5–6 days). Although the deep-level soil moisture (Fig. A1a) continues to decline throughout the simulation, this does not have an impact on fluxes to the atmosphere. Where deep-rooted vegetation is present (Figs. A1c,d), the deep-level soil water can contribute up to 50% to transpiration; however, this also coincides with areas of high annual rainfall so that deep-level soil moisture returns to an equilibrium state within six months. Radiation limits evaporation in this tropical environment at the time of the reset. Finally, in the example of shallow-rooted vegetation (Figs. A1e,f, typically occurring in semiarid areas), a response is seen in the evaporation in the days and weeks immediately after the soil moisture reset and deep soil moisture is adjusting downward throughout the simulation; however, the low contribution of the deepest-level soil moisture means that water is not removed from this level by transpiration and that this level does not contribute significantly to evaporation overall.

The period from July 1997 to the end of June 1998 has been rerun after correcting the soil moisture field.
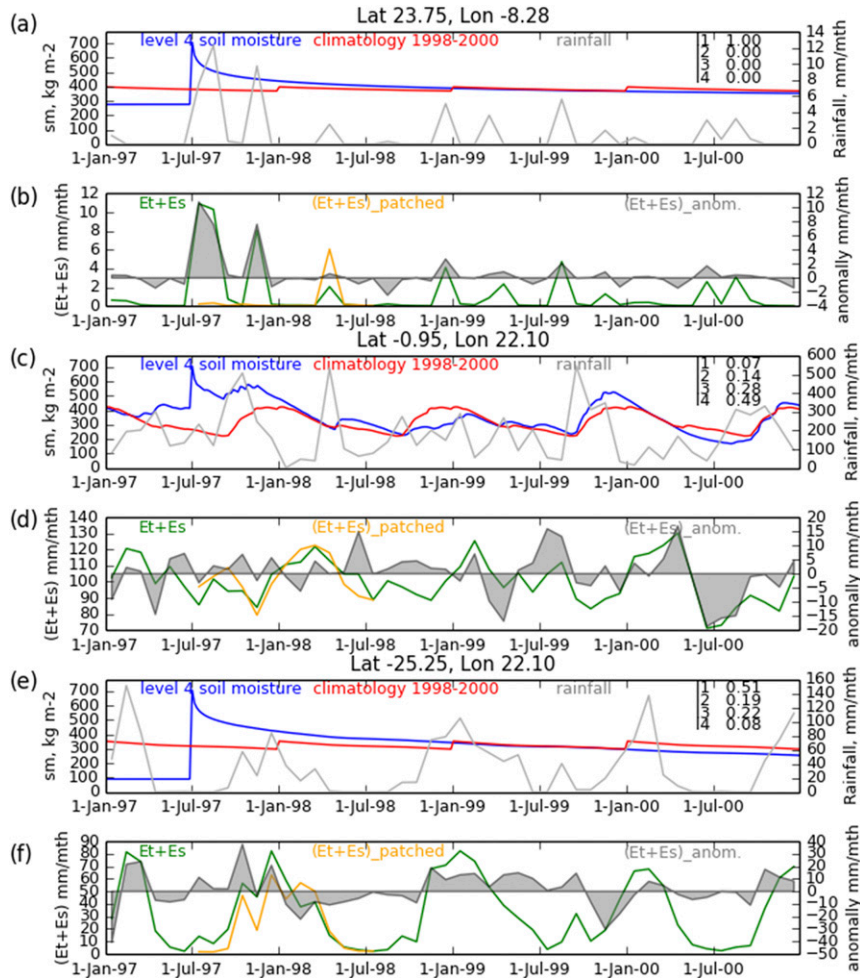
FIG. A1. Pairs of plots showing (a),(c),(e) the deep-level (level 4) soil moisture (blue) and soil moisture climatology (red) for the years 1998–2000 (kg m^{-2}), with monthly rainfall (gray; mm month^{-1}), and (b),(d),(f) monthly transpiration and bare soil evaporation and its anomaly (mm month^{-1}) for a (a),(b) bare-soil-dominated grid box, (c),(d) deep-rooted vegetation, and (e),(f) shallow-rooted vegetation.

APPENDIX B

Model Availability

The description for obtaining the model closely follows that given by Walters et al. (2017a).

a. Obtaining the UM

The Met Office Unified Model is available for use under license. A number of research organizations and national meteorological services use the UM in collaboration with the Met Office to undertake basic atmospheric process research, produce forecasts, develop the UM code, and build and evaluate Earth system models. Further information on how to apply for a license is available online (http://www.metoffice.gov.uk/research/modelling-systems/unified-model).

b. Obtaining JULES

JULES is available under license free of charge. Further information on how to gain permission to use JULES for research purpose is available online (https://jules.jchmr.org/content/getting-started).

c. Details of the simulations performed

The infrastructure for building and running UM–JULES simulations uses the Rose suite engine (http://metomi.github.io/rose/doc/rose.html) and scheduling using the Cylc work flow engine (https://cylc.github.io/cylc/). Both Rose and Cylc are available as part of version 3 (v3) of the GNU General Public License (GPL).

d. Obtaining data from the model simulation

Output from the model simulations will be made publically available in July 2019.

REFERENCES

Abel, S. J., and Coauthors, 2017: The role of precipitation in controlling the transition from stratocumulus to cumulus cloud in a Northern Hemisphere cold-air outbreak. *J. Atmos. Sci.*, **74**, 2293–2314, https://doi.org/10.1175/JAS-D-16-0362.1.

Adler, R., and Coauthors, 2003: The Version-2 Global Precipitation Climatology Project (GPCP) monthly precipitation analysis (1979–present). *J. Hydrometeor.*, **4**, 1147–1167, https://doi.org/10.1175/1525-7541(2003)004<1147:TVGPCP>2.0.CO;2.

Aranami, K., T. Davies, and N. Wood, 2015: A mass restoration scheme for limited-area models with semi-Lagrangian advection. *Quart. J. Roy. Meteor. Soc.*, **141**, 1795–1803, https://doi.org/10.1002/qj.2482.

Bain, C. L., K. D. Williams, S. F. Milton, and J. T. Heming, 2011: Anatomy of an observed African easterly wave in July 2006. *Quart. J. Roy. Meteor. Soc.*, **137**, 923–933, https://doi.org/10.1002/qj.812.

Bellouin, N., J. Rae, A. Jones, C. Johnson, J. Haywood, and O. Boucher, 2011: Aerosol forcing in the Climate Model Intercomparison Project (CMIP5) simulations by HadGAM2-ES and the role of ammonium nitrate. *J. Geophys. Res.*, **116**, D20206, https://doi.org/10.1029/2011JD016074.

Best, M. J., and Coauthors, 2011: The Joint UK Land Environment Simulator (JULES), model description—Part 1: Energy and water fluxes. *Geosci. Model Dev.*, **4**, 677–699, https://doi.org/10.5194/gmd-4-677-2011.

Beven, K. J., and M. J. Kirby, 1979: A physically based, variable contributing area model of basin hydrology. *Hydrol. Sci. Bull.*, **24**, 43–69, https://doi.org/10.1080/02626667909491834.

Birch, C. E., J. H. Marsham, D. J. Parker, and C. M. Taylor, 2014a: The scale dependence and structure of convergence fields preceding the initiation of deep convection. *Geophys. Res. Lett.*, **41**, 4769–4776, https://doi.org/10.1002/2014GL060493.

——, D. J. Parker, J. H. Marsham, D. Copsey, and L. Garcia-Carreras, 2014b: A seamless assessment of the role of convection in the water cycle of the West African monsoon. *J. Geophys. Res. Atmos.*, **119**, 2890–2912, https://doi.org/10.1002/2013JD020887.

——, S. Webster, S. C. Peatman, D. J. Parker, A. J. Matthews, Y. Li, and M. E. E. Hassim, 2016: Scale interactions between the MJO and the western Maritime Continent. *J. Climate*, **29**, 2471–2492, https://doi.org/10.1175/JCLI-D-15-0557.1.

Boutle, I. A., and C. J. Morcrette, 2010: Parametrization of area cloud fraction. *Atmos. Sci. Lett.*, **11**, 283–289, https://doi.org/10.1002/asl.293.

——, S. J. Abel, P. G. Hill, and C. J. Morcrette, 2014a: Spatial variability of liquid cloud rain: Observations and microphysical effects. *Quart. J. Roy. Meteor. Soc.*, **140**, 583–594, https://doi.org/10.1002/qj.2140.

——, J. E. Eyre, and A. P. Lock, 2014b: Seamless stratocumulus simulation across the turbulent gray zone. *Mon. Wea. Rev.*, **142**, 1655–1668, https://doi.org/10.1175/MWR-D-13-00229.1.

Brohan, P., J. Kennedy, I. Harris, S. Tett, and P. Jones, 2006: Uncertainty estimates in regional and global observed temperature changes: A new dataset from 1850. *J. Geophys. Res.*, **111**, 1865–1877, https://doi.org/10.1029/2005JD006548.

Brown, A., S. Milton, M. Cullen, B. Golding, J. Mitchell, and A. Shelly, 2012: Unified modeling and prediction of weather and climate: A 25-year journey. *Bull. Amer. Meteor. Soc.*, **93**, 1865–1877, https://doi.org/10.1175/BAMS-D-12-00018.1.

Bryan, G. H., and H. Morrison, 2012: Sensitivity of a simulated squall line to horizontal resolution and parameterization of microphysics. *Mon. Wea. Rev.*, **140**, 202–225, https://doi.org/10.1175/MWR-D-11-00046.1.

Chamberlain, J. M., C. L. Bain, D. F. A. Boyd, K. McCourt, T. Butcher, and S. Palmer, 2014: Forecasting storms over Lake Victoria using a high resolution model. *Meteor. Appl.*, **21**, 419–430, https://doi.org/10.1002/met.1403.

Cionni, I., and Coauthors, 2011: Ozone database in support of CMIP5 simulations: Results and corresponding radiative forcing. *Atmos. Chem. Phys.*, **11**, 11 267–11 292, https://doi.org/10.5194/acp-11-11267-2011.

Clark, D. B., and Coauthors, 2011: The Joint UK Land Environment Simulator (JULES), model description—Part 2: Carbon fluxes and vegetation dynamics. *Geosci. Model Dev.*, **4**, 701–722, https://doi.org/10.5194/gmd-4-701-2011.

Clark, P., N. Roberts, H. Lean, S. P. Ballard, and C. Charlton-Perez, 2016: Convection-permitting models: A step-change in rainfall forecasting. *Meteor. Appl.*, **23**, 165–181, https://doi.org/10.1002/met.1538.

Cullen, M. J. P., 1993: The unified forecast/climate model. *Meteor. Mag.*, **122**, 81–94.

Davies, T., 2014: Lateral boundary conditions for limited area models. *Quart. J. Roy. Meteor. Soc.*, **140**, 185–196, https://doi.org/10.1002/qj.2127.

——, M. J. P. Cullen, A. J. Malcolm, M. H. Mawson, A. Stainforth, A. A. White, and N. Wood, 2005: A new dynamical core for the Met Office's global and regional modelling of the atmosphere. *Quart. J. Roy. Meteor. Soc.*, **131**, 1759–1782, https://doi.org/10.1256/qj.04.101.

De Kauwe, M. G., C. M. Taylor, P. P. Harris, G. P. Weedon, and R. J. Ellis, 2013: Quantifying land surface temperature variability for two Sahelian mesoscale regions during the wet season. *J. Hydrometeor.*, **14**, 1605–1619, https://doi.org/10.1175/JHM-D-12-0141.1.

Edwards, J. M., and A. Slingo, 1996: Studies with a flexible new radiation code. I: Choosing a configuration for a large-scale model. *Quart. J. Roy. Meteor. Soc.*, **122**, 689–720, https://doi.org/10.1002/qj.49712253107.

Field, P. R., A. J. Heymsfield, and A. Bansemer, 2007: Snow size distribution parameterization for midlatitude and tropical ice clouds. *J. Atmos. Sci.*, **64**, 4346–4365, https://doi.org/10.1175/2007JAS2344.1.

Forbes, R., and C. Halliwell, 2003: Assessment of the performance of an enhanced microphysics parametrization scheme in the Unified Model at 1 km resolution. Met Office Internal Rep., 40 pp.

Futyan, J. M., and A. D. Del Genio, 2007: Deep convective system evolution over Africa and the tropical Atlantic. *J. Climate*, **20**, 5041–5060, https://doi.org/10.1175/JCLI4297.1.

Garcia-Carreras, L., and Coauthors, 2013: The impact of convective cold pool outflows on model biases in the Sahara. *Geophys. Res. Lett.*, **40**, 1647–1652, https://doi.org/10.1002/grl.50239.

Hastings, D. A., and Coauthors, 1999: The Global Land One-km Base Elevation (GLOBE) Digital Elevation Model, version 1.0. NOAA/National Geophysical Data Center, http://www.ngdc.noaa.gov/mgg/topo/globe.html.

Hook, S., R. C. Wilson, S. MacCallum, and C. J. Merchant, 2012: Lake surface temperature [in "State of the Climate in 2011"]. *Bull. Amer. Meteor. Soc.*, **93** (7), S18–S19.

Houze, R. A., Jr., 2004: Mesoscale convective systems. *Rev. Geophys.*, **42**, 1–43, https://doi.org/10.1029/2004RG000150.

Huffman, G. J., and Coauthors, 2007: The TRMM Multisatellite Precipitation Analysis (TMPA): Quasi-global, multiyear, combined-sensor precipitation estimates at fine scale. *J. Hydrometeor.*, **8**, 38–55, https://doi.org/10.1175/JHM560.1.

——, R. F. Adler, D. T. Bolvin, and E. J. Nelkin, 2010: The TRMM multi-satellite precipitation analysis (TMPA). *Satellite Rainfall Applications for Surface Hydrology*, F. Hossain and M. Gebremichael, Eds., Springer-Verlag, 3–22.

Joyce, R. J., J. E. Janowiak, P. A. Arkin, and P. Xie, 2004: CMORPH: A method that produces global precipitation estimates from passive microwave and infrared data at high spatial and temporal resolution. *J. Hydrometeor.*, **5**, 487–503, https://doi.org/10.1175/1525-7541(2004)005<0487:CAMTPG>2.0.CO;2.

Kendon, E. J., N. M. Roberts, H. J. Fowler, M. J. Roberts, S. C. Chan, and C. A. Senior, 2014: Heavier summer downpours with climate change revealed by weather forecast resolution model. *Nat. Climate Change*, **4**, 570–576, https://doi.org/10.1038/nclimate2258.

Klingaman, N. P., G. M. Martin, and A. Moise, 2017: ASoP (v1.0): A set of methods for analyzing scales of precipitation in general circulation models. *Geosci. Model Dev.*, **10**, 57–83, https://doi.org/10.5194/gmd-10-57-2017.

Kummerow, C., W. Barnes, T. Kozu, J. Shine, and J. Simpson, 1998: The Tropical Rainfall Measuring Mission (TRMM) sensor package. *J. Atmos. Oceanic Technol.*, **15**, 809–817, https://doi.org/10.1175/1520-0426(1998)015<0809:TTRMMT>2.0.CO;2.

Laing, A. G., and J. M. Fritsch, 1993: Mesoscale convective complexes in Africa. *Mon. Wea. Rev.*, **121**, 2254–2263, https://doi.org/10.1175/1520-0493(1993)121<2254:MCCIA>2.0.CO;2.

Laprise, R., L. Hernandez-Diaz, K. Tete, L. Sushama, L. Separovic, A. Martynov, K. Winger, and M. Valin, 2013: Climate projections over CORDEX Africa domain using the fifth-generation Canadian Regional Climate Model (CRCM5). *Climate Dyn.*, **41**, 3219–3246, https://doi.org/10.1007/s00382-012-1651-2.

Lean, H. W., P. A. Clark, M. Dixon, N. M. Roberts, A. Fitch, R. Forbes, and C. Halliwell, 2008: Characteristics of high-resolution versions of the Met Office Unified Model for forecasting convection over the United Kingdom. *Mon. Wea. Rev.*, **136**, 3408–3424, https://doi.org/10.1175/2008MWR2332.1.

Lewis, P., and Coauthors, 2012: The ESA globAlbedo project: Algorithm. *Int. Geoscience and Remote Sensing Symp.*, Munich, Germany, IEEE, 5745–5748, https://doi.org/10.1109/IGARSS.2012.6352306.

Lock, A. P., A. R. Brown, M. R. Bush, G. M. Martin, and R. N. B. Smith, 2000: A new boundary layer mixing scheme. Part I: Scheme description and single-column model tests. *Mon. Wea. Rev.*, **128**, 3187–3199, https://doi.org/10.1175/1520-0493(2000)128<3187:ANBLMS>2.0.CO;2.

Loeb, N. G., B. A. Wielicki, D. R. Doelling, G. L. Smith, D. Keyes, S. Kato, N. Manalo-Smith, and T. Wong, 2009: Toward optimal closure of the earth's top-of-atmosphere radiation budget. *J. Climate*, **22**, 748–766, https://doi.org/10.1175/2008JCLI2637.1.

Manners, J., S. B. Vosper, and N. Roberts, 2012: Radiative transfer over resolved topographic features for high-resolution weather prediction. *Quart. J. Roy. Meteor. Soc.*, **138**, 720–733, https://doi.org/10.1002/qj.956.

——, J. M. Edwards, P. Hill, and J.-C. Thelen, 2015: SOCRATES technical guide: Suite of Community Radiative Transfer Codes Based on Edwards and Slingo. Met Office Tech. Guide, 87 pp., http://homepages.see.leeds.ac.uk/~lecsjed/winscpuse/socrates_techguide.pdf.

Marsham, J. H., P. Knippertz, N. S. Dixon, D. J. Parker, and G. M. S. Lister, 2011: The importance of the representation of deep convection for modeled dust-generating winds over West Africa during summer. *Geophys. Res. Lett.*, **38**, L16803, https://doi.org/10.1029/2011GL048368.

——, N. S. Dixon, L. Garcia-Carreras, G. M. S. Lister, D. J. Parker, P. Knippertz, and C. E. Birch, 2013: The role of moist convection in the West African monsoon system: Insights from continental-scale convection-permitting simulations. *Geophys. Res. Lett.*, **40**, 1843–1849, https://doi.org/10.1002/grl.50347.

Martin, G. M., N. P. Klingaman, and A. F. Moise, 2017: Connecting spatial and temporal scales of the tropical precipitation in observations and the MetUM-GA6. *Geosci. Model Dev.*, **10**, 105–126, https://doi.org/10.5194/gmd-10-105-2017.

McCabe, A., R. Swinbank, W. Tennant, and A. Lock, 2016: Representing model uncertainty in the Met Office convection permitting ensemble prediction system and its impact on fog forecasting. *Quart. J. Roy. Meteor. Soc.*, **142**, 2897–2910, https://doi.org/10.1002/qj.2876.

McCaul, E. W., S. J. Goodman, K. M. LaCasse, and D. J. Cecil, 2009: Lightning threat using cloud-resolving model simulations. *Wea. Forecasting*, **24**, 709–729, https://doi.org/10.1175/2008WAF2222152.1.

Moore, R. J., 1985: The probability-distributed principle and runoff production at point and basin scales. *Hydrol. Sci.*, **30**, 273–297, https://doi.org/10.1080/02626668509490989.

Muñoz-Esparza, D., B. Kosovic, J. Mirocha, and J. Van Beeck, 2014: Bridging the transition from mesoscale to microscale turbulence in numerical weather prediction models. *Bound.-Layer Meteor.*, **153**, 409–440, https://doi.org/10.1007/s10546-014-9956-9.

Niang, I., O. C. Ruppel, M. A. Abdrado, A. Essel, C. Lennard, J. Padgham, and P. Urquhart, 2014: Africa. *Climate Change 2014: Impacts, Adaptation and Vulnerability*, V. R. Barros et al., Eds., Cambridge University Press, 1199–1265.

Nikulin, G., and Coauthors, 2012: Precipitation climatology in an ensemble of CORDEX-Africa regional climate simulations. *J. Climate*, **25**, 6057–6078, https://doi.org/10.1175/JCLI-D-11-00375.1.

Pearson, K. J., R. J. Hogan, R. P. Allan, G. M. S. Lister, and C. E. Holloway, 2010: Evaluation of the model representation of the evolution of convective systems using satellite observations of outgoing longwave radiation. *J. Geophys. Res.*, **115**, D20206, https://doi.org/10.1029/2010JD014265.

——, G. M. S. Lister, C. E. Birch, R. P. Allan, R. J. Hogan, and S. J. Woolnough, 2014: Modelling the diurnal cycle of tropical convection across the 'grey zone.' *Quart. J. Roy. Meteor. Soc.*, **140**, 491–499, https://doi.org/10.1002/qj.2145.

Poulter, B., and Coauthors, 2015: Plant functional type classification for earth system models: Results from the European Space Agency's Land Cover Climate Change Initiative. *Geosci. Model Dev.*, **8**, 2315–2328, https://doi.org/10.5194/gmd-8-2315-2015.

Prein, A. F., and A. Gobiet, 2017: Impacts of uncertainties in European gridded precipitation observations on regional climate analysis. *Int. J. Climatol.*, **37**, 305–327, https://doi.org/10.1002/joc.4706.

——, and Coauthors, 2015: A review on regional convection-permitting climate modeling: Demonstrations, prospects, and challenges. *Rev. Geophys.*, **53**, 323–361, https://doi.org/10.1002/2014RG000475.

Rayner, N. A., E. B. Horton, D. E. Parker, C. K. Folland, and R. B. Hackett, 1996: Version 2.2 of the Global sea-Ice and Sea, Surface Temperature data set, 1903-1994. Hadley Centre Tech. Note CRTN 74, 35 pp., http://hadobs.metoffice.com/gisst/crtn74.pdf.

Redelsperger, J.-L., C. D. Thorncroft, A. Diedhiou, T. Lebel, D. J. Parker, and J. Polcher, 2006: African Monsoon Multidisciplinary Analysis: An international research project and field campaign. *Bull. Amer. Meteor. Soc.*, **87**, 1739–1746, https://doi.org/10.1175/BAMS-87-12-1739.

Reynolds, R., T. Smith, C. Liu, B. Chelton, K. Casey, and M. Schlax, 2007: Daily high-resolution-blended analyses for sea surface temperature. *J. Climate*, **20**, 5473–5496, https://doi.org/10.1175/2007JCLI1824.1.

Smagorinsky, J., 1963: General circulation experiments with the primitive equations. Part 1: The basic experiment. *Mon. Wea. Rev.*, **91**, 99–164, https://doi.org/10.1175/1520-0493(1963)091<0099:GCEWTP>2.3.CO;2.

Smith, R. N. B., 1990: A scheme for predicting layer clouds and their water content in a general circulation model. *Quart. J. Roy. Meteor. Soc.*, **116**, 435–460, https://doi.org/10.1002/qj.49711649210.

Stein, T. H. M., D. J. Parker, R. J. Hogan, C. E. Birch, C. E. Holloway, G. M. S. Lister, J. H. Marsham, and S. J. Woolnough, 2015: The representation of the West African monsoon vertical cloud structure in the Met Office Unified Model: An evaluation of CloudSat. *Quart. J. Roy. Meteor. Soc.*, **141**, 3312–3324, https://doi.org/10.1002/qj.2614.

Tang, Y., H. Lean, and J. Bornemann, 2013: The benefits of the Met Office variable resolution NWP model for forecasting convection. *Meteor. Appl.*, **20**, 417–426, https://doi.org/10.1002/met.1300.

Taylor, C. M., C. E. Birch, D. J. Parker, N. Dixon, F. Guichard, G. Nikulin, and G. M. S. Lister, 2013: Modeling soil moisture-precipitation feedback in the Sahel: Importance of spatial scale versus convective parameterization. *Geophys. Res. Lett.*, **40**, 6213–6218, https://doi.org/10.1002/2013GL058511.

Tian, Y., C. D. Peters-Lidard, and J. B. Eylander, 2010: Real-time bias reduction for satellite-based precipitation estimates. *J. Hydrometeor.*, **11**, 1275–1285, https://doi.org/10.1175/2010JHM1246.1.

Van Genuchten, M. T., 1980: A closed-form equation for predicting the hydraulic conductivity of unsaturated soils. *Soil Sci. Soc. Amer. J.*, **44**, 892–898, https://doi.org/10.2136/sssaj1980.03615995004400050002x.

Walters, D. N., and Coauthors, 2011: The Met Office Unified Model global atmosphere 3.0/3.1 and JULES global land 3.0/3.1 configurations. *Geosci. Model Dev.*, **4**, 919–941, https://doi.org/10.5194/gmd-4-919-2011.

——, and Coauthors, 2017a: The Met Office Unified Model global atmosphere 6.0/6.1 and JULES Global land 6.0/6.1 configurations. *Geosci. Model Dev.*, **10**, 1487–1520, https://doi.org/10.5194/gmd-10-1487-2017.

——, and Coauthors, 2017b: The Met Office Unified Model global atmosphere 7.0/7.1 and JULES global land 7.0/7.1 configurations. *Geosci. Model Dev.*, https://doi.org/10.5194/gmd-2017-291, submitted.

Webster, S., A. R. Brown, D. R. Cameron, and C. P. Jones, 2003: Improvements to the representation of orography in the Met Office Unified Model. *Quart. J. Roy. Meteor. Soc.*, **129**, 1989–2010, https://doi.org/10.1256/qj.02.133.

Weedon, G. P., G. Balsamo, N. Bellouin, S. Gomes, M. J. Best, and P. Viterbo, 2014: The WFDEI meteorological forcing data set: WATCH Forcing Data methodology applied to ERA-Interim reanalysis data. *Water Resour. Res.*, **50**, 7505–7514, https://doi.org/10.1002/2014WR015638.

Wilkinson, J. M., and F. J. Bornemann, 2014: A lightning forecast for the London 2012 Olympics opening ceremony. *Weather*, **69**, 16–19, https://doi.org/10.1002/wea.2176.

——, A. N. F. Porson, F. J. Bornemann, M. Weeks, P. R. Field, and A. P. Lock, 2013: Improved microphysical representation of drizzle and fog for the Met Office Unified Model. *Quart. J. Roy. Meteor. Soc.*, **139**, 488–500, https://doi.org/10.1002/qj.1975.

Williams, K. D., and A. Bodas-Salcedo, 2017: A multi-diagnostic approach to cloud evaluation. *Geosci. Model Dev.*, **10**, 2547–2566, https://doi.org/10.5194/gmd-10-2547-2017.

——, and Coauthors, 2017: The Met Office Global Coupled model 3.0 and 3.1 (GC3 and GC3.1) configurations. *J. Adv. Model. Earth Syst.*, **10**, 357–380, https://doi.org/10.1002/2017MS001115.

Wilson, D. R., and S. P. Ballard, 1999: A microphysically based precipitation scheme for the UK Meteorological Office Unified Model. *Quart. J. Roy. Meteor. Soc.*, **125**, 1607–1636, https://doi.org/10.1002/qj.49712555707.

——, A. C. Bushell, A. M. Kerr-Munslow, J. D. Price, and C. J. Morcrette, 2008: PC2: A prognostic cloud fraction and condensation scheme, I: Scheme description. *Quart. J. Roy. Meteor. Soc.*, **134**, 2093–2107, https://doi.org/10.1002/qj.333.

Wood, N., and P. J. Mason, 1993: The pressure force induced by neutral, turbulent flow over hills. *Quart. J. Roy. Meteor. Soc.*, **119**, 1233–1267, https://doi.org/10.1002/qj.49711951402.

——, and Coauthors, 2014: An inherently mass-conserving semi-implicit semi-Lagrangian discretization of the deep-atmosphere global nonhydrostatic equations. *Quart. J. Roy. Meteor. Soc.*, **140**, 1505–1520, https://doi.org/10.1002/qj.2235.

Xie, P., R. Joyce, S. Wu, S.-H. Yoo, Y. Yarosh, F. Sun, and R. Lin, 2017: Reprocessed, bias-corrected CMORPH global high-resolution precipitation estimates from 1998. *J. Hydrometeor.*, **18**, 1617–1641, https://doi.org/10.1175/JHM-D-16-0168.1.

Zerroukat, M., 2010: A simple mass conserving semi-Lagrangian scheme for transport problems. *J. Comput. Phys.*, **229**, 9011–9019, https://doi.org/10.1016/j.jcp.2010.08.017.